

Magnetic Fields of Accreting X-Ray Pulsars with the *Rossi X-Ray Timing Explorer*

W. Coburn^{1,2}, W. A. Heindl², R. E. Rothschild², D. E. Gruber², I. Kreykenbohm³, J. Wilms³, P. Kretschmar^{4,5}, R. Staubert³

ABSTRACT

Using a consistent set of models, we parameterized the X-ray spectra of all accreting pulsars in the *Rossi X-ray Timing Explorer* database which exhibit Cyclotron Resonance Scattering Features (CRSFs, or cyclotron lines). These sources in our sample are Her X-1, 4U 0115+63, Cen X-3, 4U 1626-67, XTE J1946-274, Vela X-1, 4U 1907+09, 4U 1538-52, GX 301-2, and 4U 0352+309 (X Per). We searched for correlations among the spectral parameters, concentrating on how the cyclotron line energy relates to the continuum and therefore how the neutron star B -field influences the X-Ray emission. As expected, we found a correlation between the CRSF energy and the spectral cutoff energy. However, with our consistent set of fits we found that the relationship is more complex than what has been reported previously. Also, we found that not only does the width of the cyclotron line correlate with the energy (as suggested by theory), but that the width scaled by the energy correlates with the depth of the feature. We discuss the implications of these results, including the possibility that accretion directly affects the relative alignment of the neutron star spin and dipole axes. Lastly, we comment on the current state of fitting phenomenological models to spectra in the *RXTE/BeppoSAX* era and the need for better theoretical models of the X-ray continua of accreting pulsars.

Subject headings: stars:magnetic fields – stars:neutron – X-rays:stars

1. Introduction

Accretion powered X-ray pulsars (White, Swank & Holt 1983; Nagase 1989; Bildsten et al. 1997) provide a unique laboratory for the study of matter in extremes of temperature and magnetic as well as gravitational fields. After more than two decades of research, however, there is still no compelling model for the generation of the hard X-ray spectrum in these objects. This reflects the difficulties and complexities of radiative transport and magnetohydrodynamics in the environment found at the neutron star magnetic polar caps.

The observed hard X-ray emission from these objects originates primarily from one or two “hotspots” found at the neutron star magnetic poles. Due to their large magnetic fields ($B \gtrsim 10^{12}$ G), material accreted from a nearby companion couples to the neutron star B -field at several hundred neutron star radii. The material is then channeled onto the neutron star surface, forming accretion structures at the two poles. It

¹Space Sciences Laboratory, University of California at Berkeley, Berkeley, CA, 94702-7450, USA

²Center for Astrophysics and Space Sciences, University of California at San Diego, La Jolla, CA, 92093-0424, USA

³Institut für Astronomie und Astrophysik, Astronomie, University of Tübingen, Sand 1, D-72076, Tübingen, Germany

⁴INTEGRAL Science Data Center, 6 ch. d’Écogia, CH-1290 Versoix, Switzerland

⁵Max-Planck-Institut für Extraterrestrische Physik, Giessenbachstrasse 1, D-85740 Garching, Germany

is the combination of the beaming properties of these structures with the rotation of the star that gives rise to the pulsed emission seen by a distant observer. By analyzing the rotation-averaged spectral properties of these hotspots, we hope to improve our understanding of the physical conditions and properties of the emission regions of these accretion structures. This is also a step towards interpreting and understanding pulsar spectra as a function of neutron star rotation phase (pulse phase resolved spectroscopy).

For the analysis presented here, we focus on the effects of the magnetic field on the resulting hard X-ray spectrum. By using sources with known magnetic field strengths (from the measurement of cyclotron features) we remove one uncertainty from the class analysis. Our results, however, should also extrapolate to accreting pulsars with unknown B -field strengths. Another motivation was to provide an observational base for theoretical investigations into the production of the pulsar hard X-ray continuum, as well as to guide future calculations and simulations. The list of our sources, along with some of their properties, is given in Table 1.

To perform this analysis, we used sources where there was a direct measurement of the pulsar B -field using Cyclotron Resonance Scattering Features (CRSFs), also commonly referred to as “cyclotron lines.” These line-like spectral features arise due to the resonant scattering of photons by electrons whose energies are quantized into Landau levels by the magnetic field (Mészáros 1992). The fundamental energy where these features appear is given by

$$E_c = 11.6 \frac{B}{10^{12} \text{ G}} (1+z)^{-1} \text{ keV} \quad (1)$$

where B is the magnetic field (in Gauss) in the scattering region, and z is the gravitational redshift. The quantized energy levels of the electrons are to first order harmonically spaced, with features at $2E_c$, $3E_c$, etc. both predicted and, in some sources, observed (e.g. Heindl et al. 1999b; Santangelo et al. 1999; Cusumano et al. 1998). At sufficiently high magnetic fields, relativistic effects can introduce a slight anharmonicity in the rest frame resonant photon energies. In these cases the cyclotron energies are given by (Harding & Daugherty 1991)

$$E_c = m_e c^2 \frac{(1 + 2nB' \sin^2(\theta))^{1/2} - 1}{\sin^2(\theta)} \quad (2)$$

where $B' = B(\hbar e)/(m_e^2 c^3)$ is the magnetic field scaled to the QED field scale, n is the harmonic number, and θ is the angle of propagation of the photon relative to the magnetic field. Since these energies depend on the angle θ , the emergent spectral features are influenced heavily by the spatial distribution of electrons in the scattering region.

The dependence of θ in Eq. 2 indicates that, even at nonrelativistic energies, the CRSF energy is not the only source of information about the scattering region. From the Monte Carlo simulations of Araya & Harding (1999) and Isenberg, Lamb & Wang (1998b,a), it is found that the shape of the fundamental can be quite complex, and in general depends heavily on the details of the emission and scattering geometries, as well as the physical parameters such as the electron temperature and density in the scattering region. These features are also sometimes observed to vary as a function of rotation phase of the star (e.g. Burderi et al. 2000; Heindl & Chakrabarty 1999; Clark et al. 1990; Soong et al. 1990; Voges et al. 1982), allowing for the detailed study of a single accretion structure using pulse phase resolved spectroscopy.

In this paper we summarize spectral fits to ten accreting pulsars, and present observational evidence for the effect of the B -fields on the underlying hard X-ray continua of these pulsars. This was part of a larger analysis of *RXTE* archival data that encompassed 25 accreting pulsars in total. These ten (see Table 1) were selected due to the fact that their spectra exhibited CRSFs. They represent a complete sample of pulsars

with CRSFs in the *RXTE* database. The remaining sources, the ones without detectable cyclotron lines, will be discussed in a future publication.

In §2 we discuss the *Rossi X-ray Timing Explorer (RXTE)* satellite. In §3 we present a summary of the methodology and spectral models we used. In §4 we discuss the 10 pulsars in our sample, along with fits to their *RXTE* spectra. In §5 the results of the fitting are presented, along with a discussion of how correlations were found and the checks that were done using Monte Carlo simulations. In §6 we discuss our findings and their physical implications. Finally, in §7 we conclude with a brief summary of our primary results and discoveries.

2. The *RXTE*

All of our observations here were made using the two pointed instruments on the *RXTE*. The Proportional Counter Array (PCA, Jahoda et al. 1996) is a set of five nearly identical Xenon proportional counters (Proportional Counter Units, or PCUs) sensitive in the energy range 2–60 keV. Each detector has a geometric area of $\sim 1300 \text{ cm}^2$ and an energy resolution of 18% at 6 keV. To extend the lifetime of the instrument, the PCA often operates with one or more PCUs turned off, resulting in a reduced effective area during those observations. The High Energy X-ray Timing Experiment (HEXTE, Rothschild et al. 1998) consists of two clusters of 4 NaI(Tl)/CsI(Na) phoswich scintillation detectors (15–250 keV) that rock on and off source, alternately measuring source plus background and background flux. The physical area of each cluster is $\sim 800 \text{ cm}^2$, and the energy resolution is 16% at 60 keV. A pulse height analyzer in one of the detectors in Cluster B failed early in the mission and no longer provides any spectral information, effectively reducing the area of that cluster by 25%. Observations done before the failure are noted in the text. The PCA and HEXTE fields of view are co-aligned on-source and are collimated to the same 1° full width half maximum (FWHM) region.

The high voltage of the PCA has been changed several times during the mission, resulting in four “Gain Epochs” (Jahoda et al. 1996). The spectra presented here are primarily from PCA epoch 3, although there are two observations that were done during epoch 1 (see Table 2). Due to the relatively short duration of epoch 1, there has been less emphasis on understanding the calibration and producing background models during these periods. Therefore the observations obtained during this time have larger systematic uncertainties associated with them when compared to epoch 3 observations (see below). The gain of the HEXTE detectors has been held fixed by the automatic gain control system (Pelling et al. 1991) since launch, and therefore there is no HEXTE analogy to the PCA gain epochs.

PCA backgrounds were estimated using one of 2 background models released by the PCA instrument team, the choice of which depends on the source counting rate. The FAINT model is for source count rates below $40 \text{ cts s}^{-1} \text{ PCU}^{-1}$, while for brighter sources the SkyVLE model was used. Comparisons of the simulated and measured background spectra and light curves show that these models work well, especially below $\sim 20 \text{ keV}$ where our PCA analysis is concentrated (Jahoda et al. 1996). As mentioned above, the HEXTE clusters alternate pointing between target and nearby blank fields in order to measure, rather than model, the background.

The uncertainties in the PCA spectra, which have excellent counting statistics, are dominated by the systematic errors in the response matrix and background modeling (Wilms et al. 1999). To estimate the size of the systematic errors in the PCA version 2.43 response matrix, we analyzed observations of the Crab nebula and pulsar as recommended by the PCA team (Keith Jahoda, private communication). To fit

the Crab we used a combination of two power-laws; the first power-law was to account for the nebula flux while the second models emission from the pulsar. The 2–10 keV normalization of the second power-law was fixed to be 10% of the first (Jahoda 2000; Knight 1982). We then examined the best fit and increased the size of the systematic errors as a function of energy until we achieved a reduced χ^2 of unity. The second power-law is important in this type of analysis. Ignoring the contribution of the pulsar would have led us to estimate larger systematic errors, and the power-law index obtained for the nebula would disagree with what is observed by HEXTE.

When analyzing the results of fits to PCA data with no systematic errors applied, there is a large line-like residual starting at ~ 20 keV due the K-edge of Xenon (see Fig. 1). This is typically seen in all PCA spectra, and there are two methods to account for it (Keith Jahoda, private communication). The first is to use much larger systematic errors in this region, of order 5%. This is necessary because of the size of the residual. However, since we are interested in searching for and analyzing spectral lines in this region, we opted for the second method which ignores this part of the PCA spectra completely to avoid misinterpretation. Below 20 keV, the systematic errors used depend upon the gain epoch of the PCA during the observation. For gain epoch 3, where the calibration of the PCA is well understood, the typical systematic error at a given energy below 20 keV is 0.4%. For gain epoch 1, which was shorter and earlier in the mission, 0.8% systematic errors were required below 20 keV. The application of systematic errors to the data, although necessary, does mean that the use of the χ^2 statistic in fitting is no longer strictly valid. Still, quoting χ^2 when doing spectral fitting is a good indication of how well a model fits the data.

Unlike with the PCA, the dominant source of errors in spectra obtained with HEXTE are associated with photon counting statistics. This is due partly because the collecting area of HEXTE is much less than that of the PCA, and partly because of the lower intrinsic source fluxes in the HEXTE energy range. To this statistical limit the, HEXTE calibration is reasonably well understood and the released response matrices work well and agree with the PCA in the range of energies where the two instruments overlap. For our analysis we allowed for the overall normalization between the two instruments to vary freely, although in all cases it was within errors of what was expected.

We accumulated and analyzed the data using the standard NASA released `HEASoft` package of tools released by the High Energy Astrophysics Science Archive Research (HEASARC) Center⁶. The `HEASoft` consists of two packages, the `FTOOLS` data accumulation software, and the the `XANADU` spectral, timing, and image analysis software. The entire process of accumulating data using the `FTOOLS` is outlined in “The *RXTE* Cook Book: Recipes of Data Analysis and Reduction,” provided by the HEASARC on the *RXTE* Guest Observers website.

When determining source “goodtime” intervals, times from which to allow the extraction of source (or background) counts, we used the following data selection criteria. To avoid possible contamination from X-rays from the Earth’s limb, data was accumulated only when the satellite was pointing more than 10° above the horizon. To avoid possible contamination from activation in the detectors due to the high particle rates associated with SAA passages, we rejected data from a 30 minute interval beginning with the satellite entering the SAA. We also required that the satellite be pointing to within $0^\circ.01$ of the source position. Lastly, for faint sources and with the PCA instrument only, the electron ratio in each of the accumulated PCUs was required to be less than 0.10.

All other data accumulation steps, such as the modeling of the PCA background, modeling HEXTE

⁶See <http://heasarc.gsfc.nasa.gov/> on the world wide web

deadtime corrections, and generating response matrices, were done using the released `HEASoft` `FTOOL` appropriate for the task. For spectral analysis we used the `XSPEC` fitting package, released as part of `XANADU` in the `HEASoft` tools. I initially used version 10.00, and later when it was released version 11.0.1 (Arnaud 1996).

3. Methodology

When analyzing lines in pulsar spectra, a good model of the underlying continua is very important. Unfortunately, as mentioned in §1, there exists no convincing theoretical model for the shape of the continuum X-ray spectrum in accreting X-ray pulsars (Harding 1994, and references therein). Therefore observers are forced to use phenomenological models, with the choice of the specific form left to the observer. In the *RXTE* band (2–250 keV) these models take the general form of a power law that changes into a power-law times an exponential above a characteristic cutoff energy (White, Swank & Holt 1983), which we will refer to as either the standard X-ray continuum shape or simply the standard pulsar spectrum.

There are three primary analytic realizations of the standard pulsar continuum shape that have been used by various authors to fit X-ray pulsar spectra. The first, and the one used in this paper, is a power-law with a high-energy cutoff (PLCUT, White, Swank & Holt 1983). The analytic form of the PLCUT model is:

$$\text{PLCUT}(E) = A E^{-\Gamma} \times \begin{cases} 1 & (E \leq E_{\text{cut}}) \\ e^{-(E-E_{\text{cut}})/E_{\text{fold}}} & (E > E_{\text{cut}}) \end{cases} \quad (3)$$

where Γ is the photon index, and E_{cut} and E_{fold} are the cutoff and folding energies respectively. This form was chosen because it was particularly suited for our parameterization analysis (see below). The second is a power-law with a Fermi-Dirac form of the cutoff (FDCO, Tanaka 1986). Analytically this is given by the equation

$$\text{FDCO}(E) = A E^{-\Gamma} \frac{1}{1 + e^{(E-E_{\text{cut}})/E_{\text{fold}}}} \quad (4)$$

where Γ is the photon index and E_{cut} , E_{fold} the cutoff and folding energies, respectively. The third consists of dual power-laws with indices of opposite sign along with an exponential cutoff (NPEX, Mihara 1995). This is realized as

$$\text{NPEX}(E) = A(E^{-\Gamma_1} + BE^{+\Gamma_2})e^{-E/E_{\text{fold}}} \quad (5)$$

where Γ_1 and Γ_2 are photon indices with positive values, and E_{fold} the folding energy. As can be readily seen from Eqs. 3, 4, and 5, even though the models produce similar shapes, the details of the various functional forms make a meaningful comparison of fit parameters across models impossible. This underscores the need to use a single model consistently for all of the spectra in order to make generalizations about the sources as a class.

For the fits discussed in §4 and presented in Tables 5 and 6, we used a Modified-PLCUT model (MPLCUT). The standard PLCUT form (Eq. 3) has some definite advantages over the other models that are discussed below. Unfortunately, however, the slope of the PLCUT model has a discontinuity at the cutoff energy E_{cut} , which can create an artificial line-like feature in the spectral fit that can adversely affect fits to a CRSF (Kretschmar et al. 1997; Burderi et al. 2000; La Barbera et al. 2001; Coburn 2001). To account for this, we applied a “smoothing” function in the form of a relatively narrow ($\sigma \lesssim 0.1E_c$), shallow ($\tau \lesssim 0.1$) Gaussian shaped absorption feature (GABS, see below) at the cutoff energy. While this did not remove the discontinuity in the derivative at the cutoff energy, it did reduce the amplitude of residuals. The centroid energy of this Gaussian was allowed to vary in the fits, but fell within 0.3% (usually less) of the cutoff energy.

To model the CRSF, we used a Gaussian shaped function for the optical depth of the feature. The functional form was:

$$\text{GABS}(E) = \tau_c e^{-(E-E_c)^2/(2\sigma_c^2)} \quad (6)$$

where E_c is the energy of the resonance, τ_c is the depth of the line at the resonance, and σ_c is the width. This profile modifies the underlying continuum in the following way:

$$I_0(E) \rightarrow I_0(E)e^{-\text{GABS}(E)} \quad (7)$$

We note that, because this is an exponential of a Gaussian, the FWHM of the line is a complex function of not only the width σ_c , but also the depth τ_c . The resulting FWHM is slightly larger than the normal $2\sigma_c\sqrt{2\ln 2}$ for a given σ_c , but asymptotically approaches the standard value as τ_c goes to zero.

We also note that although the MPLCUT, FDCO, and NPEX equations all produce similar curves, there are differences, and a given pulsar spectrum might be fit well with one and poorly with the others. In fact, the MPLCUT fits to 4U 1538–52 (§4.8) and 4U 1907+09 (§4.7) are somewhat poor. Therefore our continua fits are not necessarily the best that can be achieved, and should not be considered the definitive *RXTE* measurements of these pulsar spectra.

Luckily, the choice of continuum model has little effect on the fits to the CRSFs themselves. This is illustrated in Table 3, where we present the results of fits to 2 different continuum models (the MPLCUT and FDCO) for a subset of 4 pulsars. Not only are the CRSF parameters of each source fit with the two continua consistent, there is also no systematic trend towards one continuum giving consistently larger or smaller values of E_c .

The ultimate goal of this analysis was to search for relations among the various model parameters to reveal real correlations in physical parameters in the pulsar emission regions. So before starting the analysis, we examined the systematic properties of these three models. Unfortunately none of the models gave consistently smaller uncertainties for all fit parameters, so any choice would leave some parameters less well constrained than had we used a different model. The decision to use the MPLCUT was based on 3 distinct advantages it offered. First, and certainly least important, this form has been used historically to fit pulsar spectra (e.g. White, Swank & Holt 1983). It therefore allows for the direct comparison of fit parameters of earlier observations, and a look into how things at the source might have changed (e.g. Gruber et al. 2001).

Second, the inter-parameter correlations of the other forms meant that, in general, the χ^2 valleys for those fits were relatively broad and flat. Therefore it was difficult for the fitting routines to find sets of parameters that represented a true minimum in χ^2 , resulting in fits that were slow to converge. These flat error basins also meant larger uncertainties in the fit parameters, and compared to the FDCO and NPEX models the MPLCUT consistently returned smaller error bars. Comparisons of these error valleys are shown in Figs. 2, 3, and 4.

The third and by far the most important consideration was that the MPLCUT model parameters themselves are relatively orthogonal to one another. This can be readily seen in the left hand panels of Fig. 2 and 3, which show error contours for spectral fits to the X-ray pulsar Hercules X-1. In the case of the MPLCUT the contours are “rounder,” implying a lower degree of correlation between the model parameters. In contrast, the contours when fitting with the FDCO model are quite elongated, with the axes of the ellipse at an angle to the parameter axes (see Fig. 2 and 3, right panels). The NPEX model is slightly better than the FDCO, but it is still not ideal for this type of analysis (see Fig. 4).

The problem arises when analyzing an ensemble of fits using models that exhibit such systematic correlations. Even if the underlying physical parameters are random, inferred parameters of poorly chosen models can show strongly correlated results. These correlations, however, are merely artifacts of the modeling procedure and *not* intrinsic to the data set. This also means that any real signal in the data will be suspect because of the potential for spurious results. By using a MPLCUT continuum, we have removed much of the systematic effects from the fitting process. Therefore the work presented here best reflects the underlying nature and physics of the pulsar polar emission region, and not artifacts of the fitting process itself.

4. Sources and Observations

In this section we describe our sample of 10 accreting pulsars, previous observations of CRSFs, the observations made using the *RXTE*, and the observed spectra. These pulsars have received various amounts of coverage by the *RXTE* in the first 5 years of operation. Given the size and richness of this database (over 4.2 Ms of satellite time), we instead discuss a representative subset of observations (see Table 4), chosen to be as long and continuous as possible, and with each source as bright as possible. The results of our spectral parameterizations are given in Table 5, and the remaining fit parameters (N_{H} , kT_{e} , etc.) are listed in Table 6.

4.1. Hercules X-1

Her X-1 is characterized by a 1.24 s pulse period (Tananbaum et al. 1972) and an eclipsing 1.7 d orbit (Deeter, Boynton & Pravdo 1981) with the A/F star HZ Her (Doxsey et al. 1973; Gottwald et al. 1991). In addition to the X-ray eclipses, Her X-1 also exhibits a 35 d intensity cycle due to the precession of a tilted, warped accretion disk viewed nearly edge on and which periodically obscures X-rays from the central neutron star (Petterson 1975). Recent models of the physical cause of the warping have been suggested by, for example, Shakura et al. (1999), Maloney & Begelman (1997), Pringle (1996), and Schandl & Meyer (1994). Due to this disk precession, the source exhibits a ~ 10 d “main-on” (where X-ray emission is a maximum) and a dimmer ~ 5 d “short-on”, separated by two ~ 10 d “low” states (where virtually no X-ray emission is detected). Her X-1 was the first X-ray pulsar in which a CRSF was discovered (Trümper et al. 1978), and since then this feature has been well studied. A recent analysis by Gruber et al. (2001), comparing *RXTE* observations with those of previous missions, has shown that the cyclotron resonance energy changed from ~ 34 keV to ~ 42 keV sometime between 1991 and 1993.

For the analysis here, only data taken during the peak of a main-on and out of eclipse were used. This was done to ensure that the observed spectrum represented the intrinsic neutron star polar cap emission, minimizing the effect of the accretion disk. The spectrum, along with the parameterizing fit, is shown in Fig. 5, upper left panel. In addition to a MPLCUT continuum and CRSF, the fit contains two Fe-K lines (both near the iron fluorescence energy 6.5 keV). The first line is narrow, with a 78 eV equivalent width (EW), and the second one much broader and with a larger (370 eV) EW. The broad Fe-K line is similar to the single 240 eV EW Fe-K line seen with *Ginga* (Mihara et al. 1991) during the main-on, although we find that a second, narrow line (which is at the detection limit for an Fe-K line in the PCA) is required by the *RXTE* data to get an acceptable χ^2 . Overall the fit is quite good, and we find a CRSF at $E_{\text{c}} = 40.4_{-0.3}^{+0.8}$ keV. This agrees with the analysis of Gruber et al. (2001) for the same dataset. There is no indication of a second CRSF harmonic near 80 keV, although due to the steeply falling spectrum our sensitivity to such a feature

is limited. A preliminary analysis of a *BeppoSAX* observation does, however, indicate that a harmonic might be present in the spectrum (Santangelo, private communication). There is also a small pattern in the residuals near 10 keV. This feature is only a $\pm 0.8\%$ deviation, and so while it does affect the resulting χ^2 , the fit parameters are not significantly affected. It does, however, appear systematically through ~ 10 PHA channels. This unexplained feature near 10 keV is exhibited in the spectra of many accreting X-ray pulsars, and is discussed in §6.4.

4.2. 4U 0115+63

The transient X-ray source 4U 0115+63 is an accreting X-ray pulsar with a 3.6 s pulsation period in an eccentric 24 d orbit (Bildsten et al. 1997) with the O9e star, V635 Cassiopeia (Unger et al. 1998). X-ray outbursts have been observed from 4U 0115+63 with *UHURU* (Forman, Tananbaum & Jones 1976), *HEAO-1* (Wheaton et al. 1979; Rose et al. 1979), *Ginga* (e.g. Tamura et al. 1992), and *CGRO/BATSE* (Bildsten et al. 1997), and reoccur with a separation times of one to several years. The *RXTE* has observed two outbursts of 4U 0115+63, the first in 1999 March (Wilson, Harmon & Finger 1999; Heindl & Coburn 1999), and the second in 2000 September (Coburn, Rothschild & Heindl 2000).

A CRSF in 4U 0115+63 was discovered near 20 keV by Wheaton et al. (1979) with the UCSD/MIT *HEAO-1/A4* low-energy (13–180 keV) detectors. White, Swank & Holt (1983) analyzed concurrent data from the lower energy (2–50 keV) *HEAO-1/A2* experiment and found an additional feature at ~ 12 keV, making this the first pulsar to exhibit more than a single line. We discuss here observations of the 1999 March outburst obtained with the *RXTE*. It was during this outburst that 4U 0115+63 became the first X-ray pulsar found to exhibit more than just a fundamental and single overtone CRSF (Heindl et al. 1999; Santangelo et al. 1999), with 5 features observed before the spectrum runs out of statistics (Heindl et al. 1999b).

The fit shown in Fig. 5 (upper right) consists of a MPLCUT continuum along with 4 CRSFs. This dataset has been discussed previously in Heindl et al. (1999) and Heindl et al. (1999b), and although different continuum models were used our results here are similar. Here, using a simple line shape (see Eq. 6) resulted in a CRSF energies of $16.4_{-1.0}^{+0.4}$ keV, $23.2_{-0.9}^{+0.4}$ keV, $31.9_{-0.7}^{+0.7}$ keV, and $48.4_{-1.3}^{+0.8}$ keV. The three higher harmonics (at 23, 32, and 48 keV) are roughly consistent with the hypothesis of harmonic spacing, although the fit fundamental is at too high of an energy. Analyzing the source spectrum as a function of neutron star rotation phase, Heindl et al. (1999b) found that the actual line shape is complex and poorly modeled by a Gaussian shaped absorption feature. Additionally, the authors found that the line centroids change considerably with pulse phase and are therefore difficult to model exactly using phase averaged spectroscopy.

So, while a single broad line centered at 16 keV is a good representation of the line shape (which is of primary interest here), the cyclotron energy of the magnetic field is better described as half that of the second harmonic, or $E_c = 11.6_{-0.4}^{+0.2}$ keV. In the fit there is also a pattern in the residuals near 7 keV that resembles an Fe-K line. These are very small deviations, however, and an Fe-K line is not formally required by the fit (with an *F*-test probability of 5×10^{-3}). We note that fits done by Heindl et al. (1999) and Santangelo et al. (1999, (using *BeppoSAX* observations obtained during the same outburst) do not require the addition of an Fe-K line.

4.3. Cen X-3

The eclipsing source Cen X-3 has a spin period of 4.8 s and a 2.1 d orbital period (Kelley et al. 1983) around the O6-8 supergiant V779 Cen (Krzemiński 1974; Rickard 1974; Hutchings et al. 1979). Historically the 1–40 keV spectrum has been fitted with the standard pulsar continuum, Fe-K line, and low energy absorption (White, Swank & Holt 1983). The analysis of *Ginga* data by Nagase et al. (1992) showed that the high-energy cutoff is better modeled by a broad, pseudo-Lorentzian turnover rather than by the standard e-folding energy cutoff. They did not claim a firm detection of a CRSF since the energy of the resonance ($\gtrsim 30$ keV) is near the 37 keV limit of the *Ginga* LAC detectors. A CRSF at 30 keV was discovered by Santangelo et al. (1998) and Heindl & Chakrabarty (1999) using *BeppoSAX* and *RXTE* observations.

In addition to a MPLCUT continuum and CRSF, we included an Fe-K line and low-energy absorption in the fit (see Fig. 5, middle left). The equivalent width of the Fe-K line was 141 eV, which is similar to the value obtained by Burderi et al. (2000) using observations obtained with *BeppoSAX*. The amount of low-energy absorption required, $N_{\text{H}} = (2.2 \pm 0.2) \times 10^{22} \text{ cm}^{-2}$, is consistent with the *BeppoSAX* value of $(1.95 \pm 0.03) \times 10^{22} \text{ cm}^{-2}$. As with Her X-1 we find a small yet systematic pattern in the residuals near 10 keV, although for Cen X-3 the “peak” is at a slightly higher energy.

The pulse phase average CRSF energy is $E_{\text{c}} = 30.4_{-0.4}^{+0.3}$, and is consistent with what was found with *BeppoSAX* (Santangelo et al. 1998). *RXTE* and *BeppoSAX* pulse phase resolved analyses have both revealed that the energy moves through the pulse; from $29.0_{-0.3}^{+0.4}$ keV during the pulse fall to 37.1 ± 1.7 keV during pulse rise (Heindl & Chakrabarty 1999). This type of variability is not unique to this source (other examples are Her X-1, Soong et al. 1990, and 4U 1538–52, Clark et al. 1990), although the magnitude of the variation in Cen X-3 ($\sim 20\%$) is quite large. This variability of the CRSF centroid energy implies that, as the neutron star rotates, different regions of the accretion structure are observed and different magnetic field strengths are indicated in these regions. This may be evidence for the dipole moment being significantly offset from the center of the neutron star (Burderi et al. 2000). It might be expected that this variation in the CRSF energy could artificially broaden a phase average measurement of the CRSF line width. The average emission is, however, dominated by flux from the peak of the pulse. A comparison of our fits with those of Heindl & Chakrabarty (1999) and Burderi et al. (2000) indicate that this movement did not significantly broaden the parameterization of the CRSF width σ_{c} .

4.4. 4U 1626–67

The 7.66 s pulsar 4U 1626–67 is in a binary system with the low-mass dwarf star KZ TrA. Although a complete orbital ephemeris is unknown there is evidence for a 42 min orbital period (Middleditch et al. 1981). The system has one of the lowest known mass functions for a pulsar (Levine et al. 1988), with a limit of $a_{\text{x}} \sin(i) < 8 \text{ lt-ms}$ (Shinoda et al. 1990). Optical limits on the companion’s luminosity rule out the possibility of accretion by a normal stellar wind (Chakrabarty 1998), so mass flow is most probably due to Roche lobe overflow of the companion in a very close binary system.

The spectrum presented in Fig. 5 (middle right panel) was obtained early in the *RXTE* mission, during PCA gain epoch 1. This was also before the failure of one of the pulse height analyzers in cluster B of HEXTE (see §2), so the HEXTE spectrum consists of spectral information from all 8 phoswich detectors.

Historically the hard X-ray spectrum of 4U 1626–67 has been modeled with a ~ 0.6 keV blackbody and low energy absorption in addition to the standard pulsar continuum (e.g. Pravdo et al. 1979; Kii et al. 1986),

so we allowed for these components as well. Our best fit blackbody temperature was $kT = 0.35_{-0.05}^{+0.04}$ keV. This is consistent with the *BeppoSAX* value of 0.33 ± 0.02 keV (Owens, Oosterbroek & Parmar 1997). The measured absorption column was $(1.6_{-0.7}^{+0.9}) \times 10^{22}$ cm⁻², which is consistent with the 8×10^{21} cm⁻² column measured by *BeppoSAX* (Owens, Oosterbroek & Parmar 1997). As seen previously, we find a CRSF at ~ 39 keV in the spectrum (Heindl & Chakrabarty 1999; Orlandini et al. 1998). In addition to the fundamental, we also found that the addition of a *second* harmonic significantly improves the continuum fit, with an F-Test probability of 2×10^{-13} . While this CRSF at 80_{-4}^{+16} keV is statistically significant, it is also only evidenced by the effects of its red wing on the continuum (see Fig. 5, middle right panel) and so its existence is still somewhat questionable.

4.5. XTE J1946+274

Not much is known about the transient pulsar XTE J1946+274. The source was discovered with the *RXTE*/ASM during a scan of the Vul-Cyg region on 1998 September 5. It was detected at a 2–12 keV flux level of ~ 13 mCrab (Smith & Takeshima 1998). It reached a peak of ~ 110 mCrab around 17 September 1998 (Takeshima & Chakrabarty 1998). Pulsations at 15.8 s were discovered by the *CGRO*/BATSE (Wilson et al. 1998) and were later confirmed through pointed *RXTE* observations (Smith & Takeshima 1998). There is also evidence for a ~ 80 d periodicity in the ASM lightcurve, which is most likely due to the orbital motion of the binary system (Campana, Israel & Stella 1999). A $36.2_{-0.7}^{+0.5}$ keV CRSF has been detected in the X-ray spectrum with both the *RXTE* (Coburn 2001; Heindl et al. 2001) and *BeppoSAX* (Santangelo et al. 2002).

The spectrum presented here (see Fig. 5, lower left) was obtained by summing 11 individual observations obtained over the course of about one month. Heindl et al. (2001) found that changes in the spectrum from observation to observation were consistent with changes in N_{H} of order 10%. Such variations are not unexpected during a Be/X-ray binary outburst, and they are likely not indicative of changes in the underlying continuum emission. For this reason, we concluded that, by excluding data below 8 keV, we could confidently combine the data, and fit with a MPLCUT continuum and CRSF.

4.6. Vela X-1

Vela X-1 (4U 0900–40) is an eclipsing X-ray binary with an orbital period of 8.964 d (van Kerkwijk et al. 1995) and which exhibits a pulsation period of ~ 283 s. The companion star is the B0.5Ib supergiant HD 77581, and the system is at a distance of 2.0 kpc (Sadakane et al. 1985). Due to the closeness of the binary orbit, the neutron star is deeply embedded in the strong stellar wind of its companion ($\dot{M} \sim 4 \times 10^{-6} M_{\odot} \text{ yr}^{-1}$, Nagase et al. 1986). X-rays are produced by accretion of this wind onto the neutron star surface. The X-ray luminosity is typically $L_{\text{x}} \sim 4 \times 10^{36}$ ergs s⁻¹, but can also suddenly change to less than 10% of its normal value (Inoue et al. 1984). The cause of this variability is still unknown, although it could be due to changes in the accretion rate due to variations in the stellar wind, or possibly associated with the formation of a temporary accretion disk (Inoue et al. 1984).

The X-ray spectrum of Vela X-1 is usually described by the standard accreting pulsar continuum plus an Fe-K line (Nagase et al. 1986; White, Swank & Holt 1983; Ohashi et al. 1984). Near periastron the spectrum is modified by significantly increased absorption due to a gas stream trailing the neutron star as well as circumstellar matter (Kaper, Hammerschlag-Hensberge & Zuiderwijk 1994). In addition, erratic increases in N_{H} by a factor of 10 are seen at all orbital phases (Haberl & White 1990). Evidence for a CRSF

at ~ 54 keV has been reported from the *High Energy X-ray Experiment* (HEXE) on the Mir space station (Kendziorra et al. 1992), from *Ginga* (Mihara 1995), from the *RXTE* (Kreykenbohm et al. 1999, 2002), and from *BeppoSAX* (Orlandini et al. 1998). There was further evidence that the fundamental CRSF lies at ~ 24 keV (e.g. Kendziorra et al. 1992; Mihara 1995), with the line at 54 being the second harmonic. Using a pulse phase resolved analysis, Kreykenbohm et al. (2002) have now confirmed the existence of the lower energy line.

The *RXTE* data we used here has already been discussed in detail by Kreykenbohm et al. (2002). The continuum we use here is different, however our fits to the CRSFs are consistent with the previous results. In the first half of the observation an anomalous X-ray dip was observed, lasting ~ 17 ks, and during this time no pulsations were seen (Kretschmar et al. 1999). The spectrum we present here (see Fig. 5, lower right) was accumulated after the dip, where the average counting rate was steady and pulsations were observed. We parameterized the phase average spectrum of Vela X-1 with a MPLCUT continuum and two CRSFs. To minimize the effects on the fit continuum spectrum due to the highly variable absorption column and Fe-K line, we ignored PCA data below 9 keV. However, we find that some X-ray absorption is still required by the data, with $N_{\text{H}} = (2.9_{-0.2}^{+0.3}) \times 10^{23} \text{ cm}^{-2}$. The width ($\sigma_{\text{c}} = 0.9_{-0.8}^{+0.9}$ keV) and depth ($\tau_{\text{c}} = 0.16_{-0.07}^{+1.13}$) of the fundamental CRSF are poorly constrained, although the addition of an absorption line near 24 keV gives an F -test probability of 1.14×10^{-7} for a chance improvement.

4.7. 4U 1907+09

The X-ray source 4U 1907+09 was discovered with the *UHURU* satellite (Giacconi et al. 1971), while observations with *Tenma* revealed the source to be a pulsar with a 437.5 s period (Makishima et al. 1984). Recent *RXTE* observations have produced an improved binary orbital ephemeris (in’t Zand, Baykal & Strohmayer 1998), along with the discovery of X-ray dips (in’t Zand, Strohmayer & Baykal 1997). The neutron star is powered by wind accretion from either a close OB supergiant (Schwartz et al. 1980) or possibly a Be star (Iye 1986; Roberts et al. 2001), and is in a close orbit (8.4 d) with the companion star. The light curve for our dataset is free from X-ray flares or dips, so the spectrum is not affected by possible spectral variability due to intensity variations. A CRSF at ~ 21 keV was discovered in this source by Makishima & Mihara (1992) using *Ginga* observations, while Cusumano et al. (1998) detected both the fundamental and a second harmonic at ~ 39 keV. We find a CRSF energy of 18.3 ± 0.4 keV.

Like 4U 1626–67 (§4.4), the spectrum here (see Fig. 6, upper left) was obtained before the failure of a pulse height analyzer in one of the HEXTE detectors (see §2), so spectral information from all 8 phoswich detectors is present. In addition to the standard pulsar continuum and CRSF, there is evidence for soft X-ray absorption in the range $N_{\text{H}} = (1.5 - 1.7) \times 10^{22} \text{ cm}^{-2}$ (see Schwartz et al. 1980; Marshall & Ricketts 1980; Makishima et al. 1984; Cook & Page 1987; Chitnis et al. 1993) and an Fe-K emission line. We find a column of $(2.4 \pm 0.1) \times 10^{22} \text{ cm}^{-2}$, which is larger than the historical values. We also find a narrow Fe-K line improves the fits. The residuals to this parameterization below 10 keV, however, make the interpretation of spectral features in this energy range ambiguous (see Fig. 6, upper left).

There is a large ($\pm 3\%$) pattern in these residuals that “peaks” slightly above 10 keV, making this the most pronounced case of the 10 keV feature. It is tempting to associate this with a CRSF at ~ 9 keV, making the features at 18 keV and 39 keV the second and fourth harmonics respectively (with the third harmonic absent). When we fit a line in this region, the energy centroid energy was indeed $E_{\text{c}} = 8_{-4}^{+2}$ keV. The feature is, however, quite broad ($\sigma_{\text{c}} = 7 \pm 3$ keV), and rather than appearing as a simple line it modifies the continuum

over a large portion of the energy range. Since other sources also show the limitations of the continuum models near this energy, and there is little evidence for a third CRSF harmonic in the spectrum, we conclude that this feature is a result of the continuum model and not a CRSF.

4.8. 4U 1538–52

The pulsar 4U 1538–52 is in an eclipsing system with the B0 Iab star QV Nor (Rubin et al. 1994; Corbet, Woo & Nagase 1993), with accretion proceeding through the companion’s wind rather than Roche-lobe overflow (Crampton, Hutchings & Cowley 1978). The source was first detected with the *UHURU* satellite (Giacconi et al. 1974), with coherent ~ 530 s pulsations later found in data from *Ariel V* (Davison, Watson & Pye 1977). The binary orbital ephemeris is well known, with an orbital period of 3.7 d (Clark 2000).

A CRSF was discovered with the *Ginga* satellite by Clark et al. (1990). The feature, centered at ~ 20 keV, was found to vary by $\sim 15\%$ through the pulse. There is no evidence for a ~ 40 keV harmonic in the spectrum, both phase averaged and phase resolved (Mihara 1995; Coburn 2001). The observation analyzed here (see Fig. 6, upper right) spanned nearly the entire binary orbit of the system (excepting the interval during the X-ray eclipse). We find a CRSF energy of $20.66_{-0.06}^{+0.05}$ keV in the source spectrum, with no indication of a second harmonic.

As with 4U 1907+09 (§4.7), the pattern of fit residuals below ~ 10 keV (which arise from the inability of the model to fit the 10 keV feature) make the interpretation of the spectrum in that energy range difficult. While appearing similar to the residuals seen in 4U 1907+09, the size of this deviation is smaller ($\pm 1.5\%$). As with 4U 1907+09, we allowed for another absorption line at near ~ 10 keV. However, the fit “line” was a broad feature ($\sigma_c = 11_{-2}^{+3}$) with an energy constrained to be less than 4 keV, and that acted to modify the entire continuum below ~ 20 keV. Therefore we again conclude that the pattern of residuals is due to the continuum model, and not a CRSF in the spectrum.

4.9. GX 301–2

The pulsar GX 301–2 (4U 1223–62) is a wind fed neutron star in a 41.5 day eccentric ($e = 0.47$) orbit around the supergiant companion Wray 977 (Sato et al. 1986). Pulsations from GX 301–2 were first detected by White et al. (1976) at ~ 700 s. The pulsar undergoes regular flares ~ 1.4 d before periastron passage, along with a smaller flare near apastron (Pravdo & Ghosh 2001; Koh et al. 1997; Pravdo et al. 1995). The primary flare is probably due to passage through the mass outflow from the companion star which is directed primarily perpendicular to its rotational axis. The X-ray spectrum is characterized by a large and variable absorption column and a strong Fe-K line (Leahy & Matsuoka 1990; Leahy et al. 1989; White & Swank 1984).

There was a suggestion of a CRSF in this source at 35.6 ± 1.6 keV using observations obtained with the *Ginga* satellite at a reduced high-voltage, extending the spectral range out to 60 keV (Makishima & Mihara 1992; Mihara 1995). But due to uncertainties in the background subtraction above 36 keV and limited high energy statistics, the detection of the CRSF was not firm (Makishima & Mihara 1992). Also, using *HEAO-1/A4* data during a source flare, Rothschild & Soong (1987) reported a possible absorption line at ~ 24 keV with an F-Test probability of 10^{-2} . With the *RXTE* we have been able to confirm the presence of a CRSF

in the spectrum, and we find a centroid energy of $E_c = 42.4_{-2.5}^{+3.8}$ keV. A CRSF has also been observed with the *BeppoSAX*, but at a higher (49.5 ± 1.0 keV) energy. (Orlandini & Fiume 2001).

The *RXTE* spectrum in Fig. 6 (lower left) was obtained during a normal, non-flaring state of GX 301–2. The low-energy absorption measured with the *RXTE* is quite large, with $N_H = (2.8 \pm 0.1) \times 10^{23}$ cm⁻². This is larger than what was observed with *Tenma* (Leahy & Matsuoka 1990) and *Ginga* (Mihara 1995), although as mentioned above the low-energy absorption column is known to be highly variable. It is this large N_H that gives rise to the edge seen in the inferred photon spectrum of the source (see Fig. 6, lower left). The *RXTE* spectrum also exhibits a prominent Fe-K line, with an 1.1 keV EW. Like other accreting pulsars there is an indication of a systematic residual centered near 10 keV ($\sim \pm 0.5\%$).

4.10. 4U 0352+309 (X Per)

The X-ray source 4U 0352+309 is an unusually low luminosity (4.2×10^{34} ergs s⁻¹) pulsar in a system with the Be star X Persei (X Per). It is also unusual in the sense that while most Be/X-ray binary systems are transient in nature, 4U 0352+309 is a source of persistent X-ray emission. This is perhaps due to the relatively wide and nearly circular orbit of the system (Delgado-Martí et al. 2001). Its ~ 837 s pulsation period was discovered with the *UHURU* satellite (White et al. 1976; White, Mason & Sanford 1977), and is still one of the longest periods of any known accreting pulsar. The distance to the system, based on optical observations of the companion X Per, is 0.95 ± 0.20 kpc (Telting et al. 1998).

A CRSF at $28.6_{-1.7}^{+1.5}$ keV was discovered in this source by Coburn et al. (2001). The spectrum, both here and in the previous work, is the sum of 40 pointings (see Table 1 of Coburn et al. 2001) spanning from 1998 July 1 through 1999 February 27, and the authors discuss in detail the validity of summing these observations. We found that, while the spectrum of 4U 0352+309 is not well fit by the standard pulsar continuum, it can be modeled successfully by a blackbody plus a power-law modified by a CRSF. In these fits we fixed the neutral absorption to be 1.5×10^{21} cm⁻², based on measurements from satellites with significant response below 1 keV (for example *ROSAT*, Haberl 1994; Mavromatakis 1993, *BBXRT*, Schlegel et al. 1993, *Copernicus*, Mason et al. 1976, and *BeppoSAX*, Di Salvo et al. 1998). As in previous observations of the source we found no evidence of an Fe-K line in the spectrum, with a 90% confidence upper limit on the equivalent width of 13 eV for a Gaussian line centered at 6.4 keV and with a 0.5 keV sigma. This is consistent with the ~ 6 eV upper limit of Di Salvo et al. (1998).

Although the existence of a high energy cutoff in the spectrum is only suggestive, for this work we used a PLCUT model in the same way as we used the MPLCUT the other sources. Since the cutoff itself was barely supported by the data, we were unable to apply our smoothing technique. Since the cutoff itself had a minimal affect on the other fit parameters, this is unlikely to be a problem for this source. When we let the PLCUT model fit, we found cutoff and folding energies of $E_{\text{cut}} = 57_{-17}^{+12}$ and $E_{\text{fold}} = 50_{-30}^{+107}$ respectively. These, along with the other parameters associated with this fit, are the values listed in Tables 5 and 6.

5. Analysis

With all of the phase averaged spectra fit in a consistent way with the same model (except 4U 0352+309 which did not require a high energy cutoff), we can now discuss any observed correlations and what these imply for the physical parameters in the pulsar polar regions. The spectral shape parameterizations are

given in Table 5, and the magnetic fields as measured by their cyclotron lines in Table 7. Of particular interest is how the CRSF parameters (E_c , σ_c , τ_c) relate to the continuum (Γ , E_{cut} , E_{fold}), and thus how the standard pulsar spectrum is affected by the magnetic field.

To identify the major linear correlations in our dataset (the 6 shape parameters for each of the 10 source spectra), we conducted a correlation analysis (e.g. Bevington & Robinson 1992). The results of which are given in Table 8. This prescription does not account for the uncertainties on each point, so these numbers should merely be used as a guide on where to search in the data. The coefficient for uncorrelated data is 0, while a perfect correlation/anticorrelation results in 1/−1 respectively. In Table 8 we see that the primary interdependence is between the CRSF line centroid energy and width (shown in bold) with a $\sim 2\%$ chance that this is due to a random signal in the data.

There are 2 sources in our analysis whose continua are slightly different from the other 8 pulsars: 4U 0352+309 and 4U 1626–67. Although 4U 0352+309 has a CRSF similar to the rest of the pulsars presented here, it has a continuum which is quite unlike the standard pulsar spectral shape. In Coburn et al. (2001) we argue that, because of its very low accretion rate, a thermal component that is normally buried by accretion is partially revealed. Also, due to inefficient cooling with lower densities, the break in the spectrum is at a much higher energy, $E_{\text{cut}} \gtrsim 50$ keV. For 4U 1626–67, a pulse phase resolved spectral analysis reveals that the cutoff energy changes from ~ 6 keV to ~ 27 keV through the pulse (see Coburn 2001). Another reason why these two sources might be different is that in both cases the binary systems are viewed nearly face on, while 6 of the remaining 8 are known to be viewed nearly edge on (see Table 1).

While we have not excluded either of these sources from the overall analysis, when we exclude both 4U 1626–67 and 4U 0352+309 from the correlation analysis a new dependency becomes apparent (see Table 9). There is now an association between the MPLCUT cutoff energy E_{cut} and the CRSF line energy, with a $\sim 0.5\%$ probability of the correlation being due simply to chance. Additionally, the connection between the CRSF width σ_c and energy E_c becomes tighter, with the same $\sim 0.5\%$ probability of a chance correlation.

Lastly, in addition to the σ_c - E_c and E_{cut} - E_c correlations, our analysis also found a new and previously unreported relation between the relative line width σ_c/E_c and the line depth τ_c . This new dependence is discussed in §6.2.

5.1. Monte Carlo Simulations

Although care has been taken to ensure that any systematic effects in the fitting procedure were minimized, other effects might be responsible for the correlations rather than the actual spectrum. These problems could be residual systematics inherent in the MPLCUT model, selection biases in finding CRSFs with satellite spectrometers, and the phenomenological nature of the continua models. In particular, both very broad and very narrow CRSFs are very difficult to identify with current instruments. Since two of our results relied on the CRSF width, we performed a series of Monte Carlo simulations to explore both the fitting process, and regions of parameter space in which we were sensitive to finding CRSFs.

5.1.1. σ_c versus E_c

Our first simulation was to investigate if the observed σ_c - E_c correlation was a result of systematic correlations between the CRSF parameters. To test this we observed how a set of simulated *RXTE* spectra,

with known input parameters that formed a grid in the σ_c - E_c plane, were fit using our software and models. If there were a systematic movement of fit parameters towards a correlation in the simulations, then the result presented in §6.1 would be suspect. To implement this we simulated 6 *RXTE* spectra (each with differing depths τ_c) at each point on a 6×6 grid in the σ_c (2–10 keV) versus E_c (20–45 keV) plane. The simulated observations were 15 ks in duration and of a pulsar with a moderate flux ($F_x = 10^{-9}$ ergs cm $^{-2}$ s $^{-1}$ in 2–10 keV). This is a conservative assumption, allowing fitting systematics and not counting statistics to dominate the fitting. We fit each of the resulting 216 spectra, and then plotted σ_c versus E_c . As expected there was some movement in the fit values from the original grid points, however there was no systematic trend towards a correlation in the data. Therefore it is safe to conclude that the correlation between σ_c and E_c is not an artifact of how our 10 pulsar spectra were fit or the model used.

The next simulation was done to see how selection biases might account for the observed correlation. Given the difficulties in identifying shallow lines, especially at higher energies, a priori one would expect some bias in the data. Using the same 15 ks observations, we simulated 30 spectra at each point on a 11×17 grid in the σ_c (1–12 keV) versus E_c (16–50 keV) plane. We fit each of the resulting spectra initially without a CRSF, and then noted the change in χ^2 upon adding one to the model. The dotted line in Fig. 7 shows the contour corresponding to $\Delta\chi^2$ of 9.21 (99% confidence for two degrees of freedom, Lampton, Margon & Bowyer 1976), with the hatched area indicating regions where a CRSF is indistinguishable from the continuum.

This “non-detection” region is easily understood. Broad features, especially at high energies where the continuum is falling steeply and statistics are running out, are nearly impossible to identify given the phenomenological nature of the continuum models. And while the red wing of broad CRSFs at these energies will affect the continuum where the statistics are better, it again becomes a question of distinguishing between a real cyclotron feature and the choice of continuum. Also, narrow lines at all energies are difficult to detect given the finite energy resolution of not just the *RXTE*, but essentially all hard X-ray satellite instruments so far.

Although the boundary does follow the trend in the data, its exact position depends on both the source flux and the length of the observation. As either increases, so will the ability to resolve lines at higher energies and thus move the dotted line to the right. Therefore it is unlikely that the absence of narrow lines at high energies can be completely explained as a selection effect. Also, selection effects cannot account at all for the lack of broad lines at lower energies.

5.1.2. Relative σ_c versus τ_c

To test for systematic effects in the CRSF depth versus relative width correlation, we again performed Monte Carlo simulations. We first simulated six 15 ks long *RXTE* spectra with CRSFs at various energies on a 6×6 grid in the σ_c/E_c (0.05–0.3) versus τ_c (0.1–1.1) plane. We then fit each of the resulting 216 spectra. Again, although there was scatter in the fit values away from the initial grid points, there was no systematic movement that could explain the observed correlation.

To test for a selection bias we next simulated 30 spectra at each point on a 11×12 grid ($0.05 \leq \sigma_c/E_c \leq 0.3$, $0.05 \leq \tau_c \leq 0.8$), each with a CRSF at 30 keV. We fitted each of the resulting spectra without a CRSF, and noted the improvement (or lack thereof) in χ^2 after the addition of an absorption line to the model. The resulting $\Delta\chi^2$ of 9.21 (99% confidence for two degrees of freedom, Lampton, Margon & Bowyer 1976) contour is plotted as a dotted line in Fig. 8, with the hatched regions indicating where the observations were not sensitive to the presence of a CRSF in the spectrum. The region along the x -axis, narrow features at all

depths, is simply due to the finite spectral resolution of the HEXTE phoswich detectors. The region that follows the y -axis, shallow features at all widths, arises from the difficulties in distinguishing shallow CRSFs from the continuum. The dotted line (along with the shaded areas) is meant as a guide to the eye, and some minor movement is inevitably due to changes in the CRSF energy or shape of the underlying continuum. The observed correlation between relative width σ_c/E_c and depth τ_c cannot, however, be explained merely in terms of either model biases or selection effects. Therefore it is safe to conclude that this is a real, physical effect.

6. Results

In this section we discuss the results found in the data analysis of §5. These are: correlations between the cyclotron width σ_c and energy E_c (§6.1), between the ratio σ_c/E_c with the cyclotron depth τ_c (§6.2), and between the cutoff energy E_{cut} with the cyclotron energy E_c (§6.3). At the end of this section we briefly discuss some possible implications of the spectral feature near 10 keV.

6.1. σ_c versus E_c

In Fig. 7 we plot the fit values of CRSF width σ_c versus energy E_c . This correlation, although not new (Heindl et al. 1999a; Dal Fiume et al. 2000), is both somewhat expected from theory and yet still surprising to observe.

The electrons in the scattering region, although quantized perpendicular are free to move parallel to the magnetic field, and therefore constitute a 1-dimensional gas (Mészáros 1992). For cold electrons the observed CRSF width would be nearly a δ -function. If, however, the electron is moving with a velocity component v_{\parallel} parallel to the field, then for a photon to be resonantly scattered it must be at the CRSF energy in the electron rest frame. Therefore, in the laboratory frame the resonance energy is $E' = E_c[1 - (v/c) \cos(\theta)]$, and depends on the photon propagation angle with respect to the B -field. For a Maxwell-Boltzmann distribution of electrons, the observed CRSF FWHM is given by Mészáros (1992):

$$\Gamma_c \propto E_c \sqrt{kT_e} |\cos(\theta)| \quad (8)$$

Where kT_e is the characteristic electron temperature, E_c the cyclotron resonance energy, and θ the viewing angle with respect to the magnetic field. This gives a very straightforward dependence of the CRSF width σ_c on energy E_c as observed in Fig. 7. There is, however, a term involving the viewing angle θ . At small angles to the magnetic field ($\cos(\theta) \sim 1$), the motions of the electrons along the magnetic field lines will result in a maximal Doppler broadening of the feature, while at large angles ($\cos(\theta) \ll 1$) the effects of thermal broadening are small and the line is expected to be very narrow.

What is unusual about the correlation seen here is that the systems should a priori be viewed at *random* values of $\cos(\theta)$, and thus smear out the correlation (the dependence on kT_e , which is much weaker, is discussed below). Therefore this implies that for sources where CRSFs are observed there is an observational bias towards a specific viewing angle θ . Interestingly, 6 of the 10 CRSF systems discussed here are also among the few accreting X-ray pulsars that exhibit eclipses (Her X-1, Cen X-3, Vela X-1, and 4U 1538–52) or are thought to be viewed nearly edge on based on fits to their orbital light curves (GX 301–2, 4U 1907+09). Also, since the angular momentum from the accreted material will seek to align the neutron star spin with that of the binary plane, knowledge of the inclination angle of the systems specifies (or nearly so) the pulsar

spin axes. This combination of a selection on a narrow range of viewing angles θ , with a bias towards systems with a large inclination, implies that there is a preferred offset angle between the dipole and spin axes.

This could be an indication as to why CRSFs have not been observed in sources such as 2S 1417–624, GS 1843+00, and GS 1843–024, where observational limitations such as source brightness and integration length were not a factor (see Coburn 2001). The orientation of their binary planes, and therefore our view of the polar emission regions, are apparently not favorable to the detection of CRSFs. This also implies that should the inclination angles of 4U 0115+63, XTE J1946+274, and A0535+26 be measured, it will be found that they are observed nearly edge on.

Given the limited number of sources in our sample and lack of theoretical work in this area, it is difficult to put an exact number or even range on what this offset angle between spin and rotation axis is. In the work of Blum & Kraus (2000) for Her X-1, this offset angle was found to be $\sim 18^\circ$. This would suggest a “small” angle, of less than $\sim 30^\circ$. However, we note that Scott, Leahy & Wilson (2000) find that for Her X-1 the angle between the spin and B -field axes is much larger (48°), although in their model the angle between the rotation and binary axes is quite large as well (52°).

Using a toy model, Wang (1981) and Wang & Robnik (1982) predict that the angle between the spin and magnetic dipole axis should change in response to accretion. This is due to a net torque on the dipole moment resulting from the accreted angular momentum. This torque will act to align the two axes during episodes of spin-down, and make them perpendicular during spin-up. The characteristic time scale for this alignment was estimated to be $t \sim 10^4$ yr, which is similar to the timescale for a neutron star to come into spin equilibrium with an accretion disk (Elsner, Ghosh & Lamb 1980) and much shorter than the ages of these pulsars. The authors suggest that most observed accreting X-ray pulsars began their lives as rapidly spinning ($P_{\text{spin}} \lesssim 1$ s) neutron stars, and then experienced significant spin-down due to a low initial mass transfer and the propeller effect (Illarionov & Sunyaev 1975). This is reasonable given that the range of spin periods for radio pulsars is $10^{-3} - 10^1$ s, while for accreting pulsars it is $10^{-3} - 10^5$ s. In this picture there is expected to be a bias towards small angles between the spin axis and magnetic moment provided that most neutron stars have not experienced significant spin-up torques during their lifetimes. This last assumption is probably not a safe one for most accreting X-ray pulsars; however, this model does underline the fact that accretion can affect the orientation of the dipole moment of the neutron star.

If this evolutionary scenario, or indeed any model that seeks to align the dipole and spin axes, is correct and the angle is small for most accreting pulsars, then the bias toward edge on systems can be understood as a bias toward viewing neutron stars perpendicular to their magnetic dipole moment. If, in general, the two axes are nearly aligned then the reason for not seeing CRSFs in more sources might simply be due to the distribution of inclinations of the systems. We note, however, that for any given pulsar with an unknown inclination angle, there is always the possibility that the cyclotron energy is out of the effective *RXTE* detection range.

There are three counter examples to the hypothesis that all pulsars with observable CRSFs are viewed edge on. Both 4U 0352+309 and 4U 1626–67 exhibit CRSFs, and yet both binary systems are viewed nearly face on (Delgado-Martí et al. 2001; Chakrabarty 1998). However, the single peak hard X-ray pulsation profiles of 4U 1626–67 (e.g. Coburn 2001) and 4U 0352+309 (e.g. Delgado-Martí et al. 2001) are consistent with viewing a single polar cap that never completely disappears behind the limb of the neutron star. This might be expected from a source viewed nearly along the spin axis, and whose magnetic dipole moment is nearly perpendicular to the spin axis. Under the right circumstances, one pole could be partially (or even completely) hidden through the pulse and the other pole viewed nearly edge-on, as with the edge-on sources

in our sample. Still, while this might explain why we observe CRSFs in these sources, it does not address why they might be orthogonal rotators. It seems unlikely that 4U 0352+309 in particular, which already has one of the longest spin periods known, was spun-up from an even longer period as required by the models of Wang (1981) and Wang & Robnik (1982).

The third counter example is the eclipsing X-ray pulsar OAO 1657–415, where so far a CRSF has eluded detection. When fit with the MPLCUT continuum, the CRSF energy implied from the cutoff energy is ~ 26 keV (see §6.3). A feature at this energy with a depth greater than $\tau_c \sim 0.2$ can be excluded at the $3\text{-}\sigma$ level for CRSF widths broader than $0.2E_c$.

The observed correlation between σ_c and E_c is quite broad, and this might be due in part to the phase averaged spectrum arising from a range of $\cos(\theta)$ for each source. This effect, while certainly present, is not expected to be large for two reasons. First, due to the viewing geometry it is unlikely that the observed range in θ for a given source is a full 90° . Instead our view of the polar region will be a smaller subset as the neutron star rotates. Second, for most of the sources in question the pulsation profile at the CRSF energy is a relatively simple single pulse. As noted for Cen X-3, the emission from the peak of this main pulse will dominate the phase average spectrum, further reducing the effective range of $\cos(\theta)$ sampled. Future pulse phase resolved fits, using phases chosen to isolate a specific $\cos(\theta)$, will test this result and produce a much tighter correlation if Eq. 8 is valid.

Assuming that Eq. 8 is correct, then the existence of the correlation also indicates a small range of temperatures in the cyclotron scattering region despite more than 3 orders of magnitude spread in luminosity (or alternatively, mass accretion rate onto the neutron star surface). As matter falls onto the polar cap it forms an accretion structure, where in steady state the amount of matter falling in balances the matter spreading out at the base. The small spread in temperatures seen could indicate that the mound parameters such as area, density profile, etc., naturally find steady state values that produce a narrow range of electron temperatures in the scattering region, irrespective of mass accretion rate.

The small range in electron temperatures can also be explained if the temperature itself is tied to the magnetic field strength. In numerical simulations by Lamb, Wang & Wasserman (1990) of isotropic injection into an optically thick plasma dominated by cyclotron line cooling and heating, the temperature is found to vary as $kT_e \sim E_c/4$. These simulations were originally done assuming the hard power-law spectra of γ -ray bursts, and therefore are not directly applicable to the softer continua of accreting X-ray pulsars. Still, such a dependence of electron temperature kT_e on the magnetic field is consistent with the observed correlation between the cyclotron energy and width. The statistics of the data are such that fits to the correlation in Fig. 7 are unable to distinguish between the two scenarios; with $\sigma_c \propto E_c$ being marginally preferred over $\sigma_c \propto E_c^{1.5}$ (substituting $kT_e \propto E_c$ in Eq. 8), but not at a statistically significant level.

Araya & Harding (1999) cite two caveats to the use of equation 8 to infer the electron temperature and viewing angle. The first is that a relativistic treatment of the scattering produces asymmetric broadening of the line even at $\theta = 90^\circ$. Second, Monte Carlo simulations indicate that the line profiles of the fundamental can be quite complex (Araya-Góchez & Harding 2000). The relativistic cross sections for resonant scattering of photons depend on the angle of photon propagation to the magnetic field. Since the distribution of scattered photons is isotropic, the effect of the angular dependence of the cross section is a non-isotropic angular redistribution of photons. Although these simulations preserve the general sense of Eq. 8, with lines at higher energies being broader, these other effects make a detailed inference of the electron temperature in terms of the CRSF width problematic.

6.2. Relative σ_c versus τ_c

In Fig. 8 we have plotted the relative CRSF width σ_c/E_c versus the optical depth τ_c . This is a much tighter correlation than σ_c versus E_c , and has not been reported before. In §6.1 we noted that as the energies of the lines increased so did their width, which can be easily understood in terms of Doppler broadening of the lines themselves. This correlation indicates that as CRSFs increase in depth, the width of the feature as a percentage of the resonance energy increases as well. Or that as CRSFs become deeper, they become broader.

This observation, that CRSFs become relatively broader as they become deeper is, in fact, *opposite* of what is expected from the relativistic cross sections alone (Araya & Harding 1999). In the calculations of the cross sections, resonant photons that travel perpendicular to the magnetic field have a greater chance of scattering (and giving rise to a deeper line) than those propagating along the field. Conversely, off resonance photons traveling parallel to the B -field are more likely to scatter than those perpendicular. This combination gives cross sections that move from shallow and broad to narrow and deep as a function of photon propagation angle. Since the correlation shown here is in the opposite sense, other factors such as angular redistribution of photons and photon spawning must be important in the formation of observed CRSFs. Indeed, in simulations of Araya-Góchez & Harding (2000), the predicted shape of the fundamental CRSF can be quite complex and depends greatly on the magnetic field strength, photon injection and scattering geometries, and viewing angle. Whether or not the Monte Carlo simulations can reproduce this result is unclear (R. Araya, private communication), and needs to be studied further.

It is interesting to note that the shallow fundamental CRSF of Vela X-1 was until recently considered controversial (Kreykenbohm et al. 2002). In Fig. 8 it is on the threshold of detectability for relatively short integration times (15 ks in HEXTE for the purposes of the simulations), and therefore might easily be indistinguishable from the continuum in a given dataset. This could explain why it has been seen in some observations (e.g. Mihara 1995; Kretschmar et al. 1997; Kreykenbohm et al. 1999, 2002) and not in others (e.g. Orlandini et al. 1998).

6.3. E_{cut} versus E_c

Our third result is a relationship between the cutoff energy E_{cut} and the CRSF energy E_c (see Fig. 9). A relationship between the two parameters was first noticed by Makishima & Mihara (1992) and later refined by Makishima et al. (1999). There, however, the authors used CRSF energies obtained with several different instruments and derived using a variety of continuum models. To find the PLCUT cutoff energies, the authors used fits to *Ginga* observations without a CRSF, and compared them to values of the CRSF energy found in the literature often from non-contemporaneous observations. They found that the relationship was consistent with a power law, $E_{\text{cut}} \propto E_c^{0.7}$, indicating a saturation as compared to a linear correlation. Our work has the advantage that each point is derived from a uniform model fit to a single spectrum. Also, with the exception of A0535+26, all points are from the *RXTE* instruments.

As indicated by the dotted line in Fig. 9 which represents $E_{\text{cut}} \propto E_c^{0.7}$, our results confirm the relationship for CRSF energies below ~ 35 keV. Above 35 keV, however, there is an indication of a change in slope in the correlation. Specifically, the cutoff energies of Cen X-3, XTE J1946+274, Her X-1, and A0535+26 are the same within errors. If real, this flattening of E_{cut} is more abrupt than the rather smooth turnover of the $E_c^{0.7}$ power law. It also suggests that the relation between the cyclotron and cutoff energies can instead be described by two linear relations, one below ~ 35 keV and one above.

While the complex correlation between the CRSF energy and the cutoff energy implies that the spectral break is related to the B -field, it is not necessarily a magnetic effect. A similar yet physically distinct possibility is that the break is a function of another physical parameter, such as the electron temperature kT_e . It may be this intermediate quantity that is proportional to the magnetic field, up to a saturation point.

Another interesting observation is that the change in slope occurs at ~ 35 keV, where the cyclotron energy is $\sim 7\%$ of the rest mass of the electron. The roll over might be an indication that relativistic effects in the creation of the continuum, are beginning to become important at those fields. This is, however, highly speculative. Whatever the cause, future models of accreting X-ray pulsar spectra will need to reproduce this correlation between the cyclotron line depth and relative width.

For illustrative purposes we have included the results of fits to *CGRO/OSSE* data for the source A0535+26 (indicated with a triangle in Fig. 9, Grove et al. 1995). Due to the high energy threshold of OSSE, for this fit the continuum was modeled with a PLCUT with E_{cut} set to zero. Therefore, we have used the cutoff energy observed by Kendziorra et al. (1994) with HEXE. Both Grove et al. (1995) and Kendziorra et al. (1994) find a suggestion of a feature near ~ 55 keV, although as was the case for Vela X-1 the existence of this as the fundamental is considered somewhat controversial. If the fundamental is at 55 keV then this is consistent with the observed correlation, while if it is at 110 keV then it significantly strengthens the already apparent saturation.

Not shown in this plot is the source 4U 0352+309, which has a cutoff energy lower limit of $E_{\text{cut}} = 60$ keV. However, as we mentioned in §4.10, the spectrum of 4U 0352+309 is unusual when compared to other accreting X-ray pulsars. The pulse phase resolved spectrum of 4U 1626–67 is different as well. In particular, the cutoff energy E_{cut} is a strong function of pulse phase, changing by a factor of 4.5 through the pulse. This change in the cutoff energy as a function of rotation phase is unlike what is seen in other sources, and therefore it is not surprising that the phase average value for this source does not fall on the observed correlation.

The third point that lies off of the correlation is GX 301–2. It is interesting to notice, however, that there is less discrepancy if the fundamental CRSF lies *not* at 42 keV, but instead at 21 keV as suggested by Rothschild & Soong (1987). This may be an indication that the fundamental feature, as in Vela X-1, is shallow and difficult to detect. Since the CRSF parameters of energy, width, and depth are known to change with pulse phase, a full pulse phase resolved analysis could answer this question. Unfortunately the archival HEXTE data was obtained in a mode where such an analysis is impossible. Recent *RXTE* observations, however, should answer this question (I. Kreykenbohm, private communication).

Since we are inferring the effect of the magnetic field on the standard pulsar continuum, we have plotted two values of 4U 0115+63 CRSF centroid energy. The higher value (plotted as a diamond) is the result of the parameterization used here, and is the center of the absorption feature as modeled with the GABS analytic form. The second (plotted as a circle) is at half the energy of the second harmonic, and therefore is a better estimate of the pulsar magnetic field (see §4.2). We did not make this distinction in the previous 2 sections because those were investigations into the CRSF shapes themselves, and the shape of the CRSF in 4U 0115+63 as parameterized with the GABS model is centered at ~ 16 keV. Here, however, since the CRSF energy is used to measure the B -field the distinction is necessary.

6.4. The Feature at 10 keV

One interesting feature in most of these MPLCUT fits is the wiggle, or “bump,” in the spectrum in the range 8–12 keV. It might easily be mistaken for a CRSF, especially given the size of the residuals in, for example, the spectrum of 4U 1907+09 (see Fig. 6, upper left). However, these features cannot be fit with simple absorption line models. This wiggle is evident in the spectra of many accreting X-ray pulsars, including those that do not otherwise exhibit a CRSF (e.g. GS 1843+00, see Coburn 2001). While it often appears as a simple dip, it can also evidence itself as a pure bump (e.g. Her X-1, see §4.1) or a pseudo-P-Cygni profile. Since this bump is consistently at or near 10 keV, irrespective the CRSF energy, the feature is probably not a magnetic effect.

The bump is not just apparent in *RXTE* spectra either. In Mihara (1995), the residuals in fits using the NPEX model to *Ginga* observations (e.g. 4U 1538–52, 4U 1907+09, and V0331+53) show a systematic structure around 10 keV (Mihara 1995). Pulse phase resolved spectroscopy indicates that the feature changes through the pulse. This ~ 10 keV bump is also evident in the residuals seen with the *BeppoSAX* High Pressure Gas Scintillation Proportional Counter (HPGSPC) in Cen X-3 (Santangelo et al. 1998). Since this feature has been seen in a number of sources by several satellites, and yet is not present in the observed spectra of other sources (like the Crab nebula/pulsar) it is safe to conclude that it is an inherent feature in the spectra of accreting pulsars.

The shape of the feature seen in plots of residuals almost certainly arises from modeling the continuum with a simple power-law (MPLCUT) or nearly a power-law (FDCO) below the cutoff energy. This improper modeling may also account for the different patterns of residuals that are observed, rather than physical changes in the conditions creating the feature. The NPEX model, with two components that each have an independent normalization, can mimic this feature somewhat. Still, as seen in Mihara (1995), the model is only marginally successful at accounting for the feature for most sources.

While it could be safely ignored in previous missions, the large collecting area of the PCA, which is 50% larger than the previously largest proportional counter flown (the *Ginga* LAC), has made this spectral “feature” something that can no longer be ignored. As the collecting areas of satellite spectrometers become larger, this problem will continue to hinder accurate spectral modeling. Therefore we strongly encourage the development of theoretical models for accreting X-ray pulsar spectra that can be compared directly with the observations and reduce the reliance on the currently used phenomenological models.

7. Summary

There are three principle results of this class analysis of the spectra and cyclotron features of accreting X-ray pulsars. The first two results involve correlations among the shape parameters of the CRSFs themselves. We find that the observed CRSF widths are roughly proportional to their energy. If the widths are primarily due to Doppler broadening, then this implies a viewing angle selection bias in finding sources that exhibit cyclotron features. Since 6 of the 10 sources discussed here are in systems that are viewed nearly edge on, a selection bias on viewing angles further suggests a preferred offset angle between the dipole and spin axes of the neutron star.

The next result is that, at least for the fundamental features, deeper CRSFs are also broader, even when scaled by the centroid energy. This is difficult to understand simply in terms of the relativistic cross sections alone, which are in the *opposite* sense. This implies that other effects, such as photon spawning or

the non-isotropic angular redistribution of photons, are important and should continue to be considered in theoretical efforts.

Lastly, we find a correlation between the magnetic field strength and the spectral cutoff energy. The existence of a correlation indicates that the observed spectral break is either a magnetic effect, or perhaps is tied to the magnetic field through some intermediate quantity. In the correlation itself there is a departure from the power-law observed by Makishima et al. (1999), either a roll over or break in the slope, near a cyclotron resonance energy of 35 keV. This might be an indication that the break is indeed tied to another quantity, such as the electron temperature, that is then tied to the magnetic field up to a saturation point.

We also discussed a departure in observed pulsar spectra from the standard pulsar continuum shape. While the standard shape is still applicable over most of the hard X-ray band, modern satellites have shown that it is inadequate near 10 keV. This highlights the need for theoretical work in how the X-ray continuum in these pulsars is formed, and when fitting spectra a departure away from the purely phenomenological models currently being used.

This work was supported by NASA grant NAS5-30720, NSF Travel Grant NSF INT-9815741, LTSA Grant NAG5-10691, and DAAD travel grants.

REFERENCES

- Araya, R. A., & Harding, A. K., 1999, *ApJ*, 517, 334
- Araya-Góchez, R. A., & Harding, A. K., 2000, *ApJ*, 544, 1067
- Arnaud, K. A., 1996, in *ASP Conf. Ser. 101: Astronomical Data Analysis Software and Systems V*, ed. G. H. Jacoby, J. Barnes, Vol. 5, 17
- Bevington, P. R., & Robinson, D. K., 1992, *Data reduction and error analysis for the physical sciences*, (New York: McGraw-Hill), 2nd edition
- Bildsten, L., et al., 1997, *ApJS*, 113, 367
- Blum, S., & Kraus, U., 2000, *ApJ*, 529, 968
- Burderi, L., Di Salvo, T., Robba, N. R., La Barbera, A., & Guainazzi, M., 2000, *ApJ*, 530, 429
- Campana, S., Israel, G., & Stella, L., 1999, *A&A*, 352, L91
- Chakrabarty, D., 1998, *ApJ*, 492, 342
- Chitnis, V. R., Rao, A. R., Agrawal, P. C., & Manchanda, R. K., 1993, *A&A*, 268, 609
- Clark, G. W., 2000, *ApJ*, 542, L131
- Clark, G. W., Woo, J. W., Nagase, F., Makishima, K., & Sakao, T., 1990, *ApJ*, 353, 274
- Coburn, W., 2001, *Ph.D. thesis*, University of California, San Diego, La Jolla, CA
- Coburn, W., Heindl, W. A., Gruber, D. E., Rothschild, R. E., Staubert, R., Wilms, J., & Kreykenbohm, I., 2001, *ApJ*, 552, 738

- Coburn, W., Rothschild, R., & Heindl, W. A., 2000, IAU Circular, 7487, 1
- Cook, M. C., & Page, C. G., 1987, MNRAS, 225, 381
- Corbet, R. H. D., Woo, J. W., & Nagase, F., 1993, A&A, 276, 52
- Crampton, D., Hutchings, J. B., & Cowley, A. P., 1978, ApJ, 225, L63
- Cusumano, G., Di Salvo, T., Burderi, L., Orlandini, M., Piraino, S., Robba, N., & Santangelo, A., 1998, A&A, 338, L79
- Dal Fiume, D., et al., 2000, in Broad Band X-ray Spectra of Cosmic Sources, ed. K. Makishima, L. Piro, T. Takahashi, COSPAR/Pergamon Press), 399
- Davison, P. J. N., Watson, M. G., & Pye, J. P., 1977, MNRAS, 181, 73P
- Deeter, J. E., Boynton, P. E., & Pravdo, S. H., 1981, ApJ, 247, 1003
- Delgado-Martí, H., Levine, A. M., Pfahl, E., & Rappaport, S. A., 2001, ApJ, 546, 455
- Di Salvo, T., Burderi, L., Robba, N. R., & Guainazzi, M., 1998, ApJ, 509, 897
- Doxsey, R., Bradt, H. V., Levine, A., Murthy, G. T., Rappaport, S., & Spada, G., 1973, ApJ, 182, L25
- Elsner, R. F., Ghosh, P., & Lamb, F. K., 1980, ApJ, 241, L155
- Forman, W., Tananbaum, H., & Jones, C., 1976, ApJ, 206, L29
- Giacconi, R., Kellogg, E., Gorenstein, P., Gursky, H., & Tananbaum, H., 1971, ApJ, 165, L27
- Giacconi, R., Murray, S., Gursky, H., Kellogg, E., Schreier, E., Matilsky, T., Koch, D., & Tananbaum, H., 1974, ApJS, 27, 37
- Gottwald, M., Steinle, H., Graser, U., & Pietsch, W., 1991, A&AS, 89, 367
- Grove, J. E., et al., 1995, ApJ, 438, L25
- Gruber, D. E., Heindl, W. A., Rothschild, R. E., Coburn, W., Staubert, R., Kreykenbohm, I., & Wilms, J., 2001, ApJ, 562, 499
- Haberl, F., 1994, A&A, 283, 175
- Haberl, F., & White, N. E., 1990, ApJ, 361, 225
- Harding, A. K., 1994, in The Evolution of X-ray Binaries, ed. S. Holt, C. S. Day, (New York: American Institute of Physics Press), 429
- Harding, A. K., & Daugherty, J. K., 1991, ApJ, 374, 687
- Heindl, W. A., & Chakrabarty, D., 1999, in Proceedings of the Symposium “Highlights in X-ray Astronomy in honour of Joachim Trümper’s 65th birthday”, ed. B. Aschenbach, M. J. Freyberg, Vol. 272, (Garching: Max-Planck Institute), 25
- Heindl, W. A., & Coburn, W., 1999, IAU Circular, 7126, 2

- Heindl, W. A., et al., 1999a, in *The Fifth Compton Symposium*, ed. M. L. McConnell, J. M. Ryan, Vol. 366, (New York: American Institute of Physics Press), 178
- Heindl, W. A., Coburn, W., Gruber, D. E., Pelling, M., Rothschild, R. E., Wilms, J., Pottschmidt, K., & Staubert, R., 1999b, in *The Fifth Compton Symposium*, ed. M. L. McConnell, J. M. Ryan, Vol. 366, (New York: American Institute of Physics Press), 173
- Heindl, W. A., Coburn, W., Gruber, D. E., Pelling, M. R., Rothschild, R. E., Wilms, J., Pottschmidt, K., & Staubert, R., 1999, *ApJ*, 521, L49
- Heindl, W. A., Coburn, W., Gruber, D. E., Rothschild, R. E., Kreykenbohm, I., Wilms, J., & Staubert, R., 2001, *ApJ*, 563, L35
- Hutchings, J. B., Cowley, A. P., Crampton, D., van Paradijs, J., & White, N. E., 1979, *ApJ*, 229, 1079
- Illarionov, A. F., & Sunyaev, R. A., 1975, *A&A*, 39, 185
- Inoue, H., Ogawara, Y., Waki, I., Ohashi, T., Hayakawa, S., Kunieda, H., Nagase, F., & Tsunemi, H., 1984, *PASJ*, 36, 709
- in't Zand, J. J. M., Baykal, A., & Strohmayer, T. E., 1998, *ApJ*, 496, 386
- in't Zand, J. J. M., Strohmayer, T. E., & Baykal, A., 1997, *ApJ*, 479, L47
- Isenberg, M., Lamb, D. Q., & Wang, J. C. L., 1998a, *ApJ*, 493, 154
- Isenberg, M., Lamb, D. Q., & Wang, J. C. L., 1998b, *ApJ*, 505, 688
- Iye, M., 1986, *PASJ*, 38, 463
- Jahoda, K., 2000, in *Rossi2000: Astrophysics with the Rossi X-ray Timing Explorer*
- Jahoda, K., Swank, J. H., Giles, A. B., Stark, M. J., Strohmayer, T., Zhang, W., & Morgan, E. H., 1996, *SPIE*, 2808, 59
- Kaper, L., Hammerschlag-Hensberge, G., & Zuiderwijk, E. J., 1994, *A&A*, 289, 846
- Kelley, R. L., Rappaport, S., Clark, G. W., & Petro, L. D., 1983, *ApJ*, 268, 790
- Kendziorra, E., et al., 1994, *A&A*, 291, L31
- Kendziorra, E., et al., 1992, in *The Compton Observatory Science Workshop*, (Goddard Space Flight Center: NASA), 217, see N92-21874 12-90
- Kii, T., Hayakawa, S., Nagase, F., Ikegami, T., & Kawai, N., 1986, *PASJ*, 38, 751
- Knight, F. K., 1982, *ApJ*, 260, 538
- Koh, D. T., et al., 1997, *ApJ*, 479, 933
- Kretschmar, P., Kreykenbohm, I., Wilms, J., Staubert, R., Heindl, W. A., Gruber, D. E., & Rothschild, R. E., 1999, in *The Fifth Compton Symposium*, ed. M. L. McConnell, J. M. Ryan, Vol. 366, (New York: American Institute of Physics Press), 163
- Kretschmar, P., et al., 1997, *A&A*, 325, 623

- Kreykenbohm, I., Coburn, W., Wilms, J., Kretschmar, P., Staubert, R., Heindl, W. A., & Rothschild, R. E., 2002, Phase-resolved Spectroscopy of Vela X-1, A&A in press
- Kreykenbohm, I., Kretschmar, P., Wilms, J., Staubert, R., Kendziorra, E., Gruber, D., Heindl, W. A., & Rothschild, R., 1999, A&A, 341, 141
- Krzemiński, W., 1974, ApJ, 192, L135
- La Barbera, A., Burderi, L., Di Salvo, T., Iaria, R., & Robba, N. R., 2001, ApJ, 553, 375
- Lamb, D. Q., Wang, J. C. L., & Wasserman, I. M., 1990, ApJ, 363, 670
- Lampton, M., Margon, B., & Bowyer, S., 1976, ApJ, 208, 177
- Leahy, D. A., & Matsuoka, M., 1990, ApJ, 355, 627
- Leahy, D. A., Matsuoka, M., Kawai, N., & Makino, F., 1989, MNRAS, 237, 269
- Levine, A., Ma, C. P., McClintock, J., Rappaport, S., van der Klis, M., & Verbunt, F., 1988, ApJ, 327, 732
- Makishima, K., Kawai, N., Koyama, K., Shibazaki, N., Nagase, F., & Nakagawa, M., 1984, PASJ, 36, 679
- Makishima, K., & Mihara, T., 1992, in *Frontiers of X-ray Astronomy (Proc. of the 28th Yamada Conf.)*, ed. Y. Tanaka, K. Koyama, (Tokyo: Uni. Acad. Press), 23
- Makishima, K., Mihara, T., Nagase, F., & Tanaka, Y., 1999, ApJ, 525, 978
- Maloney, P. R., & Begelman, M. C., 1997, ApJ, 491, L43
- Marshall, N., & Ricketts, M. J., 1980, MNRAS, 193, 7P
- Mason, K. O., White, N. E., Sanford, P. W., Hawkins, F. J., Drake, J. F., & York, D. G., 1976, MNRAS, 176, 193
- Mavromatakis, F., 1993, A&A, 276, 353
- Mészáros, P., 1992, *High-energy radiation from magnetized neutron stars*, (Chicago: University of Chicago Press)
- Middleditch, J., Mason, K. O., Nelson, J. E., & White, N. E., 1981, ApJ, 244, 1001
- Mihara, T., 1995, *Ph.D. thesis*, University of Tokyo
- Mihara, T., Ohashi, T., Makishima, K., Nagase, F., Kitamoto, S., & Koyama, K., 1991, PASJ, 43, 501
- Nagase, F., 1989, PASJ, 41, 1
- Nagase, F., Corbet, R. H. D., Day, C. S. R., Inoue, H., Takeshima, T., Yoshida, K., & Mihara, T., 1992, ApJ, 396, 147
- Nagase, F., Hayakawa, S., Sato, N., Masai, K., & Inoue, H., 1986, PASJ, 38, 547
- Ohashi, T., et al., 1984, PASJ, 36, 699
- Orlandini, M., et al., 1998, A&A, 332, 121

- Orlandini, M., et al., 1998, *ApJ*, 500, L163
- Orlandini, M., & Fiume, D. D., 2001, *astro-ph/0107531*
- Owens, A., Oosterbroek, T., & Parmar, A. N., 1997, *A&A*, 324, L9
- Pelling, M. R., Rothschild, R. E., MacDonald, D. R., Hertel, R., & Nishiie, E., 1991, *SPIE Proceedings*, 1549, 134
- Petterson, J. A., 1975, *ApJ*, 201, L61
- Pravdo, S. H., Day, C. S. R., Angelini, L., Harmon, B. A., Yoshida, A., & Saraswat, P., 1995, *ApJ*, 454, 872
- Pravdo, S. H., & Ghosh, P., 2001, *ApJ*, 554, 383
- Pravdo, S. H., et al., 1979, *ApJ*, 231, 912
- Pringle, J. E., 1996, *MNRAS*, 281, 357
- Rickard, J. J., 1974, *ApJ*, 189, L113
- Roberts, M. S. E., Michelson, P. F., Leahy, D. A., Hall, T. A., Finley, J. P., Cominsky, L. R., & Srinivasen, R., 2001, *astro-ph/0103140*, *ApJ* in press
- Rose, L. A., Marshall, F. E., Holt, S. S., Boldt, E. A., Rothschild, R. E., Serlemitsos, P. J., Pravdo, S. H., & Kaluziński, L. J., 1979, *ApJ*, 231, 919
- Rothschild, R. E., et al., 1998, *ApJ*, 496, 538
- Rothschild, R. E., & Soong, Y., 1987, *ApJ*, 315, 154
- Rubin, B. C., et al., 1994, in *The Evolution of X-ray Binaries*, ed. S. Holt, C. S. Day, (New York: American Institute of Physics Press), 455
- Sadakane, K., Hirata, R., Jugaku, J., Kondo, Y., Matsuoka, M., Tanaka, Y., & Hammerschlag-Hensberge, G., 1985, *ApJ*, 288, 284
- Santangelo, A., Del Sordo, S., Segreto, A., Dal Fiume, D., Orlandini, M., & Piraino, S., 1998, *A&A*, 340, L55
- Santangelo, A., et al., 1999, *ApJ*, 523, L85
- Santangelo, A., Segreto, A., Orlandini, M., Parmar, A. N., Oosterbroek, T., & Campana, S., 2002, submitted to *ApJ Letters*
- Sato, N., Nagase, F., Kawai, N., Kelley, R. L., Rappaport, S., & White, N. E., 1986, *ApJ*, 304, 241
- Schandl, S., & Meyer, F., 1994, *A&A*, 289, 149
- Schlegel, E. M., et al., 1993, *ApJ*, 407, 744
- Schwartz, D. A., Griffiths, R. E., Bowyer, S., Thorstensen, J. R., & Charles, P. A., 1980, *AJ*, 85, 549
- Scott, D. M., Leahy, D. A., & Wilson, R. B., 2000, *ApJ*, 539, 392
- Shakura, N. I., Prokhorov, M. E., Postnov, K. A., & Ketsaris, N. A., 1999, *A&A*, 348, 917

- Shinoda, K., Kii, T., Mitsuda, K., Nagase, F., Tanaka, Y., Makishima, K., & Shibasaki, N., 1990, PASJ, 42, L27
- Smith, D. A., & Takeshima, T., 1998, IAU Circular, 7014, 1
- Soong, Y., Gruber, D. E., Peterson, L. E., & Rothschild, R. E., 1990, ApJ, 348, 641
- Takeshima, T., & Chakrabarty, D., 1998, IAU Circular, 7016, 1
- Tamura, K., Tsunemi, H., Kitamoto, S., Hayashida, K., & Nagase, F., 1992, ApJ, 389, 676
- Tanaka, Y., 1986, in IAU Colloq. 89: Radiation Hydrodynamics in Stars and Compact Objects, ed. D. Mihalas, K. H. Winkler, (New York: Springer), 198
- Tananbaum, H., Gursky, H., Kellogg, E. M., Levinson, R., Schreier, E., & Giacconi, R., 1972, ApJ, 174, L143
- Telting, J. H., Waters, L. B. F. M., Roche, P., Boogert, A. C. A., Clark, J. S., de Martino, D., & Persi, P., 1998, MNRAS, 296, 785
- Trümper, J., Pietsch, W., Reppin, C., Voges, W., Staubert, R., & Kendziorra, E., 1978, ApJ, 219, L105
- Unger, S. J., Roche, P., Negueruela, I., Ringwald, F. A., Lloyd, C., & Coe, M. J., 1998, A&A, 336, 960
- van Kerkwijk, M. H., van Paradijs, J., Zuiderwijk, E. J., Hammerschlag-Hensberge, G., Kaper, L., & Sterken, C., 1995, A&A, 303, 483
- Voges, W., Pietsch, W., Reppin, C., Trümper, J., Kendziorra, E., & Staubert, R., 1982, ApJ, 263, 803
- Wang, Y.-M., 1981, Space Science Reviews, 30, 341
- Wang, Y.-M., & Robnik, M., 1982, A&A, 107, 222
- Wheaton, W. A., et al., 1979, Nature, 282, 240
- White, N. E., Mason, K. O., Huckle, H. E., Charles, P. A., & Sanford, P. W., 1976, ApJ, 209, L119
- White, N. E., Mason, K. O., & Sanford, P. W., 1977, Nature, 267, 229
- White, N. E., Mason, K. O., Sanford, P. W., & Murdin, P., 1976, MNRAS, 176, 201
- White, N. E., & Swank, J. H., 1984, ApJ, 287, 856
- White, N. E., Swank, J. H., & Holt, S. S., 1983, ApJ, 270, 711
- Wilms, J., Nowak, M. A., Dove, J. B., Fender, R. P., & di Matteo, T., 1999, ApJ, 522, 460
- Wilson, C. A., Finger, M. H., Wilson, R. B., & Scott, D. M., 1998, IAU Circular, 7014, 2
- Wilson, R. B., Harmon, B. A., & Finger, M. H., 1999, IAU Circular, 7116, 1

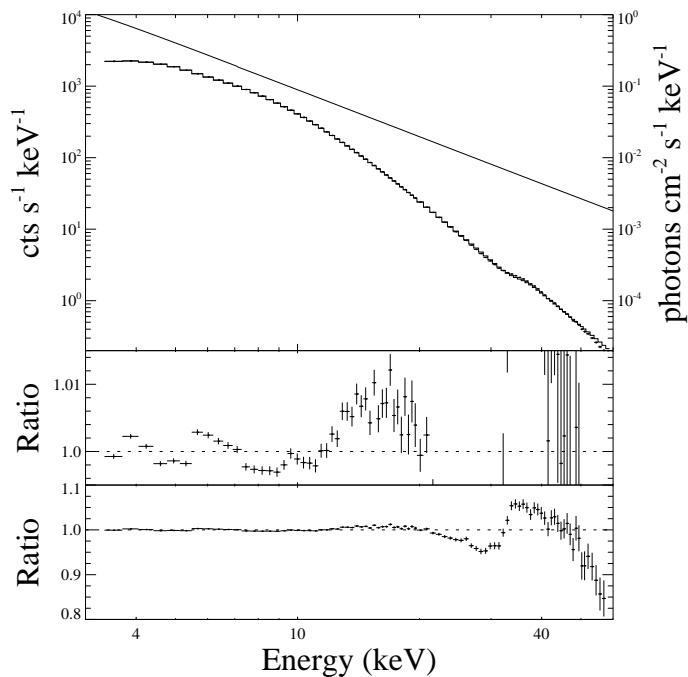


Fig. 1.— Top: A dual power-law fit to the PCA spectrum of the Crab nebula/pulsar (see text). Shown are the counts spectrum (crosses), inferred photon spectrum (smooth curve, see appropriate source section for details) and model folded through the PCA response matrix (histogram). The observations was obtained on 1996 August 23 and lasted 10ks with all 5 PCUs. The fit is using two power-laws, the first with an index of $2.245^{+0.004}_{-0.003}$, and the second with an index of $1.87^{+0.01}_{-0.02}$ and a normalization constrained to be 10% that of the first power-law. Middle: Ratio of the data to the best fit dual power-law model. Below ~ 12 keV the size of the residuals is approximately $\pm 0.4\%$. Bottom: Same plot as in the middle pane, only with an enlarged vertical scale. Due to the large line-like residual in the response matrix, we have limited our analysis of PCA data to energies below 20 keV.

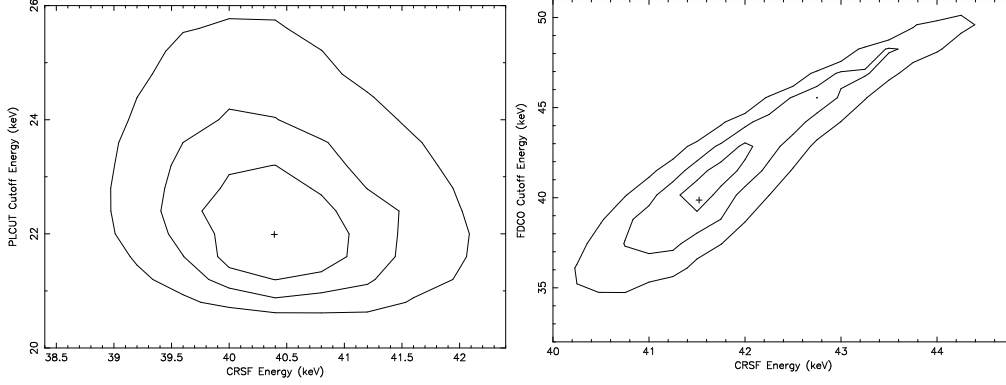


Fig. 2.— Left: Contour plot of MPLCUT cutoff energy E_{cut} versus CRSF centroid energy E_c . All plots in Figs. 2, 3, and 4 were obtained using spectral fits of Hercules X-1, and show 68%, 90%, and 99% confidence contours. Right: A similar plot using the FDCO continuum model. See § 3 for a description of the models. It is readily apparent the the two parameters are highly correlated with each other in the FDCO model, while for the MPLCUT model they are relatively independent. This aspect of the FDCO makes attempts to correlate the values obtained in spectral fitting suspect, hence our use of a modified PLCUT (MPLCUT) in the analysis presented here.

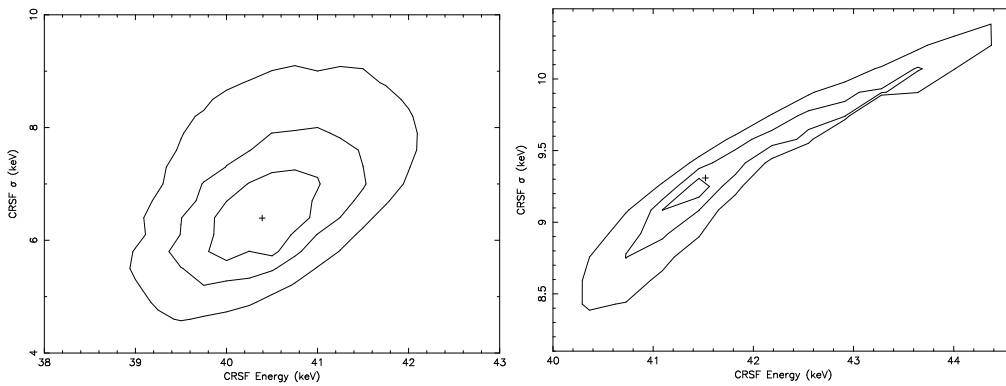


Fig. 3.— Left: Contour plot of CRSF width σ_c versus CRSF energy E_c with a MPLCUT continuum model (68%, 90%, and 99% confidence contours). Right: A similar plot using the FDCO continuum model. Again, the parameters of the FDCO model exhibit a high degree of interdependence.

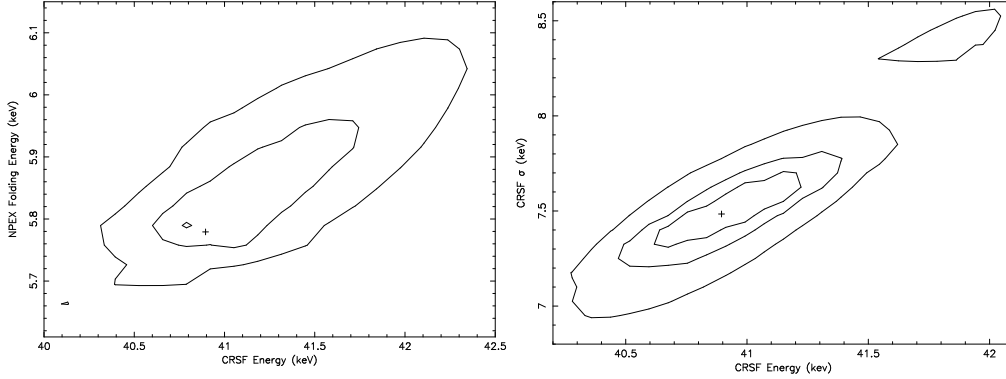


Fig. 4.— Similar contours to those above using the NPEX model, showing the 68%, 90%, and 99% confidence levels. While the contours are not as pronounced as in the FDCO model, they are still quite elongated.

Table 1: *RXTE* CRSF Sources

System	Type	P_{spin} (s)	P_{orb} (days)	Companion (MK Type)	Eclipsing
Hercules X-1	LMXB ^a	1.2377	1.70	HZ Her (A/F)	Yes
4U 0115+63	Be-Transient	3.61	24.3	V635 Cas (Be)	No
Centaurus X-3	HMXB ^b	4.82	2.09	V779 Cen (O6-8f)	Yes
4U 1626–67	LMXB	7.67	0.0289	KZ TrA	No
XTE J1946+274	Transient	15.83	–	–	No
Vela X-1	HMXB	283.2	8.96	HD 77581 (B0.5 Ib)	Yes
4U 1907+09	HMXB	440.4	8.38	(Be?)	Nearly
4U 1538–52	HMXB	528.8	3.73	QV Nor (B0 Iab)	Yes
GX 301–2	HMXB	681	41.5	Wray 977 (B1.5 Ia)	Nearly
4U 0352+309	Be-Persistent	837.7	250.3	X Per (09 III-Ve)	No

^aLow Mass X-ray Binary

^bHigh Mass X-ray Binary

Table 2: PCA Configurations During Observations (see §2)

Source	Gain Epoch	Background Model	PCUs	Layers
Her X-1	3	SkyVLE	0,1,2	Top
4U 0115+63	3	SkyVLE	0,1,2,3	Top
Cen X-3	3	SkyVLE	All	Top
4U 1626–67	1	Faint	All	Top
XTE J1946+274	3	SkyVLE	0,1,2	Top
Vela X-1	3	SkyVLE	0,1,2,4	Top
4U 1907+09	1	Faint	All	All
4U 1538–52	3	SkyVLE/Faint	0,1,2	Top
GX 301–2	3	SkyVLE	All	Top
4U 0352+309	3	SkyVLE	0,1,2	Top

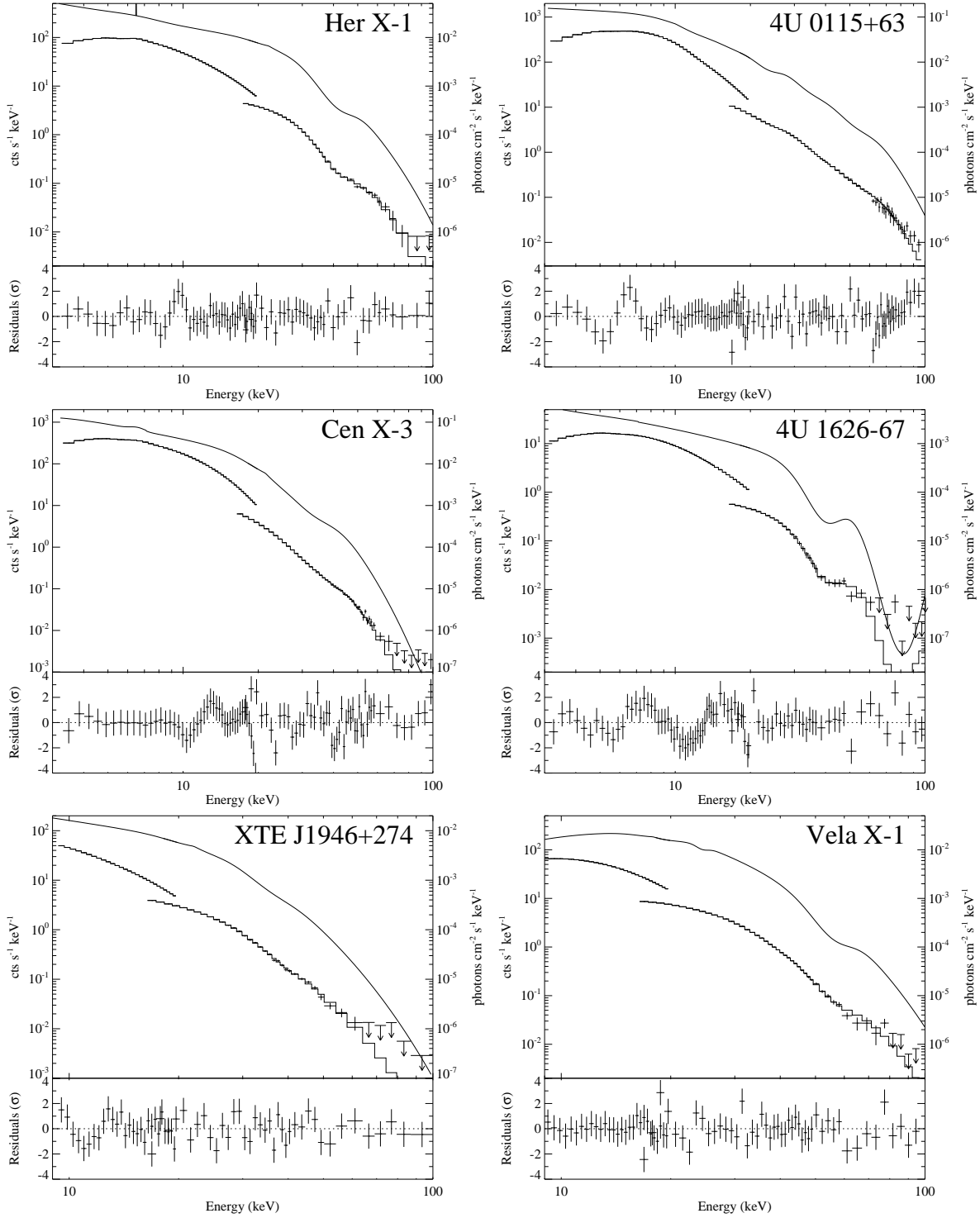


Fig. 5.— Upper Left: Her X-1. Upper Right: 4U 0115+63. Middle Left: Cen X-3. Middle Right: 4U 1626–67. Lower Left: XTE J1946+274. Lower Right: Vela X-1. All Panels: The top pane presents the counts spectrum (crosses), inferred photon spectrum (smooth curve, see appropriate source section for details) and model folded through the instrumental responses (histogram). The bottom pane contains the residuals to the fit in units of σ .

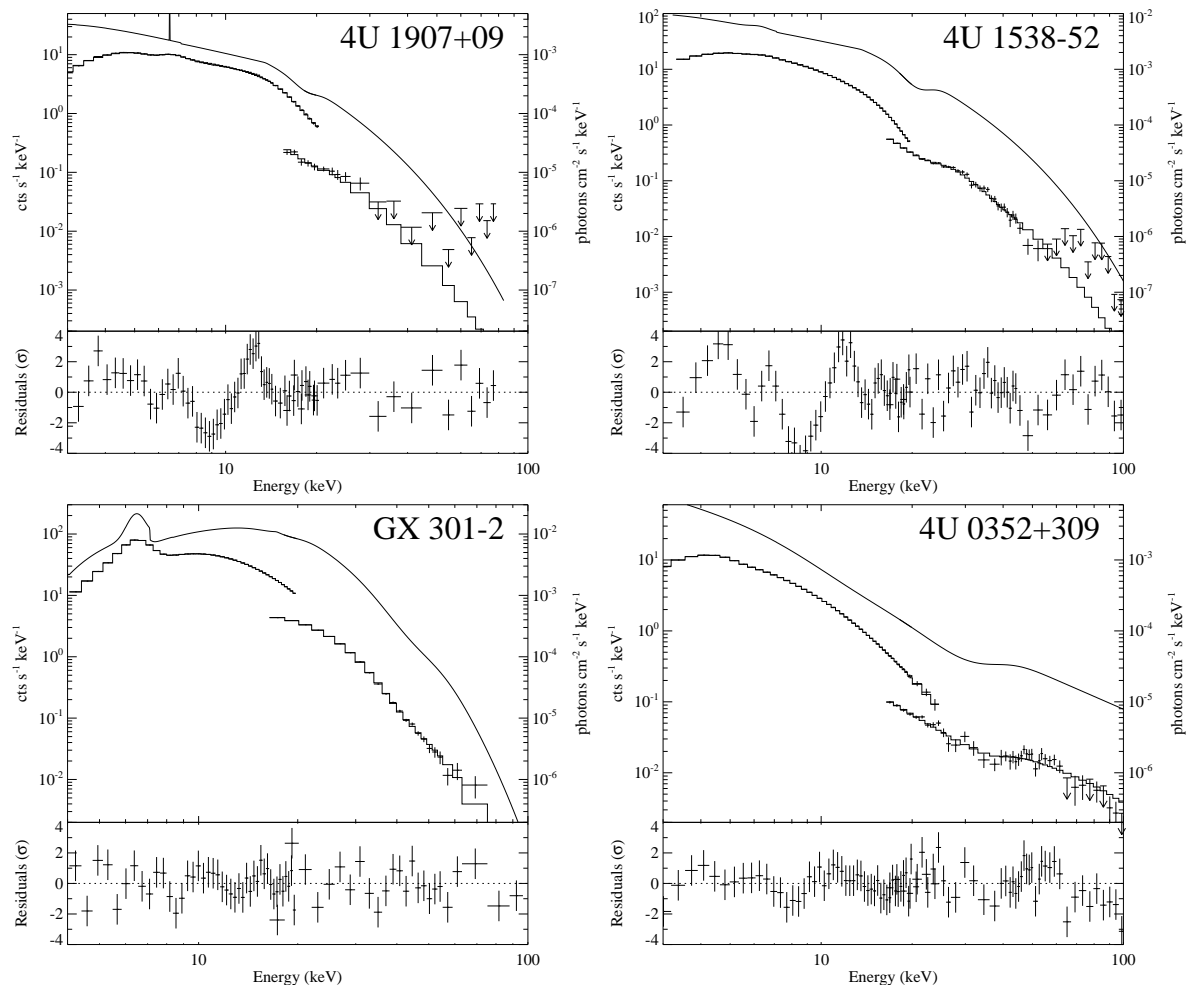


Fig. 6.— Upper Left:4U 1907+09. Upper Right: 4U 1538–52. Lower Left: GX 301–2. Lower Right:4U 0352+309. All Panels: The top pane presents the counts spectrum (crosses), inferred photon spectrum (smooth curve, see appropriate source section for details) and model folded through the instrumental responses (histogram). The bottom pane contains the residuals to the fit in units of σ .

Table 3: CRSF Fits to Different continua

Source	Continua	E_c	σ_c	τ_c
Her X-1	MPLCUT	$40.4^{+0.8}_{-0.3}$	$6.4^{+1.1}_{-0.4}$	$0.76^{+0.10}_{-0.08}$
	FDCO	$41.4^{+1.5}_{-0.3}$	$9.2^{+0.6}_{-0.1}$	$1.69^{+0.66}_{-0.07}$
Cen X-3	MPLCUT	$30.4^{+0.3}_{-0.4}$	7.1 ± 0.2	1.1 ± 0.1
	FDCO	29.9 ± 0.1	8.8 ± 0.1	1.4 ± 0.1
XTE J1946+274	MPLCUT	$34.9^{+1.9}_{-0.8}$	$4.8^{+3.2}_{-1.6}$	0.2 ± 0.1
	FDCO	$35.7^{+1.2}_{-1.1}$	3.7 ± 1.1	0.3 ± 0.1
GX 301–2	MPLCUT	$42.4^{+3.8}_{-2.5}$	$8.0^{+1.8}_{-2.6}$	$0.5^{+0.3}_{-0.2}$
	FDCO	$39.8^{+0.2}_{-3.4}$	$10.4^{+0.1}_{-4.6}$	0.4 ± 0.1

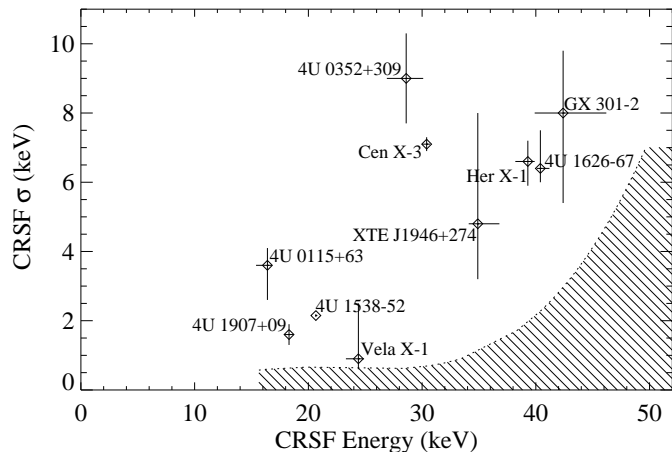


Fig. 7.— CRSF width σ_c versus centroid energy E_c . The correlation between the two parameters is obvious. The shaded region indicates a non-detection region for CRSFs based upon the results of Monte Carlo simulations (99% confidence). CRSFs in this region would not be distinguishable from the underlying continua (see, §5.1.1). The dotted line is based upon a conservative estimate of observing time and source flux. Increasing either of these parameters would allow for the detection of lines at higher energies, and would therefore move the shaded region to the right.

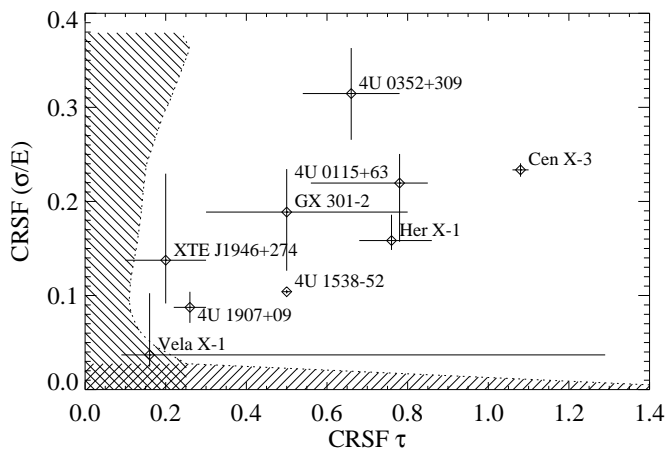


Fig. 8.— Relative CRSF width (σ_c/E_c) versus CRSF optical depth τ_c . A high degree of correlation is readily apparent in the data. As in Fig. 7, the shaded regions indicate regions in parameter space where the *RXTE* is not sensitive to CRSFs (99% confidence, see §5.1.2).

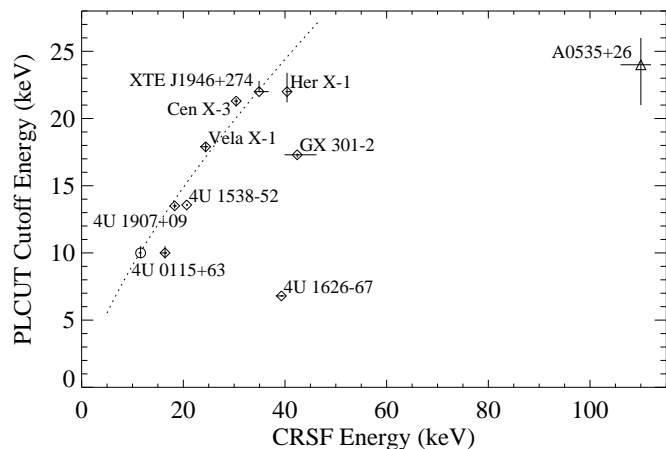


Fig. 9.— MPLCUT cutoff energy E_{cut} versus CRSF centroid energy E_c . Two CRSF energies are shown for 4U 0115+63, the diamond indicating the fit value (and therefore the center of the feature as modeled with a GABS) and a circle at 1/2 the energy of the second harmonic (and thus a is a measure of B -field, see §4.2 for details). The *CGRO*/OSSE energy (Grove et al. 1995) and HEXE cutoff (Kendziorra et al. 1994) of A0535+26 are shown as a diamond, while the lower limit for a cutoff energy in 4U 0352+309 is outside the plot. The new CRSF source XTE J1946+47, along with Cen X-3, Her X-1, and A0535+26 indicate a flattening of the power-law correlation (shown as a dotted line) observed by Makishima et al. (1999).

Table 4: Summary of Observations

Source	Date	PCA		HEXTE	
		Livetime (ks)	Rate ^a (cts s ⁻¹ PCU ⁻¹)	Livetime (ks)	Rate ^b (cts s ⁻¹ PCU ⁻¹)
Her X-1	1997 Sep 14	19.4	254.2 ± 0.2	11.9	56.2 ± 0.1
4U 0115+63	1999 Mar 3	16.7	927 ± 1	15.4	112.6 ± 0.1
Cen X-3	1997 Feb 28/Mar 2	157.3	560.4 ± 0.4	129.4	51.83 ± 0.04
4U 1626–67	1996 Feb 11–14	121.5	26.78 ± 0.02	81.8	6.49 ± 0.05
XTE J1946+274	see Heindl et al. (2001)	30.6	237.1 ± 0.1	19.7	43.0 ± 0.1
Vela X-1	1998 Jan 22	19.1	208.0 ± 0.3	11.5	120.4 ± 0.2
4U 1907+09	1996 Feb 21	18.3	18.29 ± 0.04	12.2	1.9 ± 0.2
4U 1538–52	1997 Jan 3–5	100.8	46.83 ± 0.04	62.1	5.10 ± 0.06
GX 301–2	1996 Sep 12	27.0	114.6 ± 0.08	20.6	50.1 ± 0.1
4U 0352+309	see Coburn et al. (2001)	161.4	20.55 ± 0.03	109.3	1.60 ± 0.04

^aIn the range 3–20 keV

^bIn the range 15–100 keV

Table 5: Source MPLCUT Parameterizations

Source	Γ	E_{cut}	E_{fold}	E_c	σ_c	τ_c	$\chi^2_{\text{red}}/\text{DOF}$
Her X-1	$0.93^{+0.01}_{-0.02}$	$22.0^{+1.4}_{-0.8}$	$10.8^{+0.2}_{-0.3}$	$40.4^{+0.8}_{-0.3}$	$6.4^{+1.1}_{-0.4}$	$0.76^{+0.10}_{-0.08}$	0.691/76
4U 0115+63	$0.26^{+0.10}_{-0.02}$	$10.0^{+0.5}_{-0.4}$	$9.3^{+0.5}_{-0.2}$	$16.4^{+0.4}_{-1.0}$	$3.6^{+0.5}_{-1.0}$	$0.78^{+0.07}_{-0.22}$	1.105/83
Cen X-3	$1.24^{+0.01}_{-0.02}$	$21.3^{+0.2}_{-0.4}$	$6.67^{+0.09}_{-0.06}$	$30.4^{+0.3}_{-0.4}$	7.1 ± 0.2	1.08 ± 0.02	1.536/114
4U 1626-67	0.88 ± 0.05	6.8 ± 0.3	$38.8^{+5.5}_{-4.6}$	$39.3^{+0.6}_{-1.1}$	$6.6^{+0.6}_{-0.7}$	2.1 ± 0.2	1.263/122
XTE J1946+274	$1.14^{+0.02}_{-0.03}$	$22.0^{+0.8}_{-0.9}$	$8.3^{+0.5}_{-0.4}$	$34.9^{+1.9}_{-0.8}$	$4.8^{+3.2}_{-1.6}$	0.2 ± 0.1	1.067/52
Vela X-1	$0.00^{+0.09}_{-0.01}$	$17.9^{+0.3}_{-0.4}$	$8.8^{+0.2}_{-0.1}$	$24.4^{+0.5}_{-1.1}$	$0.9^{+0.9}_{-0.8}$	$0.16^{+1.13}_{-0.07}$	0.879/64
4U 1907+09	$1.236^{+0.007}_{-0.012}$	13.5 ± 0.2	9.8 ± 0.6	18.3 ± 0.4	1.6 ± 0.2	0.26 ± 0.04	1.827/95
4U 1538-52	$1.161^{+0.003}_{-0.014}$	$13.57^{+0.04}_{-0.05}$	11.9 ± 0.1	$20.66^{+0.05}_{-0.06}$	2.15 ± 0.04	0.50 ± 0.01	2.207/116
GX 301-2	-0.02 ± 0.04	$17.3^{+0.1}_{-0.2}$	$6.7^{+0.7}_{-0.3}$	$42.4^{+3.8}_{-2.5}$	$8.0^{+1.8}_{-2.6}$	$0.5^{+0.3}_{-0.2}$	1.240/60
4U 0352+309	1.82 ± 0.02	57^{+12a}_{-17}	50^{+107a}_{-30}	$28.6^{+1.5}_{-1.7}$	9.0 ± 1.3	0.66 ± 0.12	0.876/80

^aNot required by fit

Table 6: MPLCUT Other Fit Parameters

Source	$N_{\text{H}}(10^{22} \text{ cm}^{-2})$	kT (keV)	E_{FeK} (keV)	EW_{FeK} (eV)	"Smoothing" Function		
					E (keV)	σ (keV)	τ
Her X-1	-	-	$6.0^{+0.2}_{-0.4}/6.49^{+0.03}_{-0.06}$	370/78	$22.0^{+1.3}_{-0.9}$	$3.0^{+0.3}_{-0.2}$	$0.18^{+0.05}_{-0.03}$
4U 0115+63	-	-	-	-	$11.2^{+0.4}_{-0.3}$	2.2 ± 0.3	$0.37^{+0.08}_{-0.12}$
Cen X-3	2.1 ± 0.2	-	6.51 ± 0.04	141	$21.0^{+0.3}_{-0.4}$	0.4 ± 0.4	$3.8^{+0.1}_{-0.4}$
4U 1626-67 ^a	$1.6^{+0.9}_{-0.7}$	$0.35^{+0.04}_{-0.05}$	-	-	6.8 ± 0.3	0^{+0}_{-0}	0^{+0}_{-0}
XTE J1946+274	-	-	-	-	$0.30^{+0.07}_{-0.06}$	$22.0^{+1.1}_{-1.1}$	$3.4^{+0.3}_{-0.6}$
Vela X-1	-	-	-	-	$0.28^{+0.01}_{-0.03}$	$18.5^{+0.2}_{-0.4}$	2.4 ± 0.02
4U 1907+09 ^a	2.4 ± 0.1	-	6.52 ± 0.07	175	$13.6^{0.7}_{-0.3}$	$0^{+0.3}_{-0}$	0^{+0}_{-0}
4U 1538-52 ^a	$1.98^{+0.04}_{-0.18}$	-	6.25 ± 0.06	61	$13.6^{0.3}_{-0.2}$	0^{+0}_{-0}	0^{+0}_{-0}
GX 301-2	28 ± 1	-	$6.445^{+0.007}_{-0.005}$	1100	17.6 ± 0.3	$2.30^{+0.07}_{-0.12}$	0.27 ± 0.02
4U 0352+309 ^b	0.15^c	1.44 ± 0.01	-	-	-	-	-

^aSmoothing function did not significantly affect fit

^bHigh energy cutoff not required by fit

^cFixed

Table 7: Pulsar Magnetic Fields

System	E_c keV	$B(1+z)^{-1} \times 10^{12}$ G	$B \times 10^{12}$ G ^a
Hercules X-1	$40.4^{+0.8}_{-0.3}$	3.5	4.5
4U 0115+63 ^b	$11.6^{+0.2}_{-0.4}$	1.0	1.3
Centaurus X-3	$30.4^{+0.3}_{-0.4}$	2.6	3.4
4U 1626–67	$39.3^{+0.6}_{-1.1}$	3.4	4.4
XTE J1946+274	$34.9^{+1.9}_{-0.8}$	3.0	3.9
Vela X-1	$24.4^{+0.5}_{-1.1}$	2.1	2.7
4U 1907+09	18.3 ± 0.4	1.6	2.1
4U 1538–52	$20.66^{+0.05}_{-0.06}$	1.8	2.3
GX 301–2	$42.4^{+3.8}_{-2.5}$	3.7	4.8
4U 0352+309	$28.6^{+1.5}_{-1.7}$	2.5	3.2

^aAssuming $R_{\text{ns}} = 10$ km, $M_{\text{ns}} = 1.4 M_{\odot}$, and scattering near the surface of the star

^bUsing 1/2 the energy of the second harmonic, see text

Table 8: Correlation Matrix, All Sources

	Γ	E_{cut}	E_{fold}	E_c	σ_c	τ_c
Γ	1.00	0.56	0.51	−0.08	0.28	0.12
E_{cut}		1.00	0.57	0.09	0.53	−0.21
E_{fold}			1.00	0.15	0.49	0.50
E_c				1.00	0.70	0.37
σ_c					1.00	0.46
τ_c						1.00

Table 9: Correlation Matrix, Excluding 4U 1626–67 and 4U 0352+309

	Γ	E_{cut}	E_{fold}	E_c	σ_c	τ_c
Γ	1.00	0.25	0.31	−0.11	−0.02	0.17
E_{cut}		1.00	−0.35	0.78	0.53	0.08
E_{fold}			1.00	−0.41	−0.57	−0.17
E_c				1.00	0.81	0.12
σ_c					1.00	0.60
τ_c						1.00